Università degli studi di Trento

Centre for Integrative Biology

Master of Science in Cellular and Molecular Biotechnology

In vitro **self-organization of MinD mutants**

Academic year 2014/2015

Graduant: Tassinari Andrea

External Supervisor: Prof. Petra Schwille
Internal Supervisor: Prof. Sheref S. Mansy
Tutor: Simon Kretschmer

"By itself, emergence can be no explanation at all if you don't have any insight into the mechanisms of the system, and it may seem to be an appeal to mysticism."

E. O. Wilson in an interview by Roger Lewin in *"Complexity: life at the edge of chaos"*

Abstract

Bacterial binary fission occurs upon correct placement of the division septum in the middle of the cell. Here, the tubulin homolog FtsZ polymerizes into the so-called "Z-ring" and determines the future division site. The Min system in *Escherichia coli* is fundamental in regulating cytokinesis by inhibiting Z-ring assembly at the cell poles in a spatiotemporal fashion. The system is composed of three proteins encoded by the *minB* operon: MinC is the direct inhibitor of FtsZ polymerization; MinD is a membrane-binding ATPase that oscillates from cell pole to cell pole driven by ATP consumption; MinE activates membrane detachment of MinD via stimulation of MinD's ATP hydrolysis. By oscillating together with MinD and MinE, a time-averaged concentration gradient of the FtsZ inhibitor MinC is established with minimum at midcell, where Z-ring assembly can occur.

Min protein oscillations are a biological example of self-organization, with the oscillatory pattern being an emergent property of the system resulting solely from the dynamic interactions among the components. Pattern formation by the Min system also occurs *in vitro*: when incubated on supported lipid membranes, the Min proteins self-organize into propagating planar surface waves. The *in vitro* setup represents a simple, suitable condition for the investigation of protein pattern formation at the molecular level. One question is how the biochemical features of Min proteins influence the dynamics; one way to address this goal is to make use of biochemical engineering to interfere with pattern formation and analyze the effects.

For this project, I selected six MinD protein mutants previously reported in the literature as valuable biochemical tools to study variations in Min protein self-organization. MinD L267E, L267W, and Ins3 were reported to display altered membrane affinities; MinD R3E, I4Q, and 3aaNT were suggested to present modifications in the ATPase activity. A eGFP-tagged and -untagged version of each mutant was cloned and purified. The purified mutants were then tested for their level of membrane binding, enzymatic activity, and self-organization using biochemical and biophysical techniques. In particular, MinD mutants' self-organization was qualitatively and quantitatively characterized with the use of laser scanning confocal microscopy.

One of the mutants, MinD Ins3, showed an outstanding behavior never reported so far, namely "standing waves". A deeper analysis of the patterns displayed by the mutant was performed; nevertheless, self-organization of MinD Ins3 into standing waves is a phenomenon that still deserves further studies and particular attention.

Contents

List of Figures

List of Tables

Preface

My first encounter with the thrilling world of bottom-up synthetic biology initially started in 2014, when I was given the possibility to join Prof. Petra Schwille's lab for a two month-summer research project.
As a biotechnologist, my scientific enthusiasm has always been stimulated by the ambition to identify the bare requirements and general principles of life. The underlying idea is that such thorough elucidation is both philosophically interesting and useful in applied settings.
A recent approach to better investigate basic principles of biological phenomena is to reconstitute selected subsystems from the bottom-up in well-defined biomimetic environments. Reconstituting a biological system from the bottom-up means reconstructing a functional system from scratch using a minimal set of functional elements. Toward this end, engineering concepts such as modularity and standardization are of great use. Chemistry and physics play a crucial role role as well: these disciplines aim at a quantitative understanding of life, thus informing us how a living system could function in a very simple form [1].
In the Schwille lab I could experience how different disciplines come together on a common objective. During my summer project I got familiar with some of the major biochemical and biophysical techniques used for the quantitative investigation of living systems. Coming back to the lab for my Master project, I made use of molecular engineering to elucidate the role of biochemical properties in a pattern-forming protein system reconstituted *in vitro*. Overall, I gained experience from different areas of biological investigation. And eventually I like to see my project as a small contribution to a bigger view in the framework of synthetic biology: the *in vitro* reconstitution of a self-replicating biomimetic system that fulfills the elementary requirements of life.

Chapter 1

Introduction

1.1 Self-organization and pattern formation

Self-organization is a process in which a new property at the global level of a system emerges solely from the local interactions among the lower-level composing elements of the system. Importantly, this emergent property cannot be deduced from the individual characteristics of the components alone, but is the result of their collective dynamic behavior. The emergent, global-level property of the system can be defined as "pattern": "a particular, organized arrangement of objects in space or time" [2]. Self-organization leading to pattern formation occurs in a variety of systems (Fig. 1.1). Examples in the natural world include the colorful pigmentation patterns of tropical fish, the collective behavior of ant colonies, and wind-blown sand assembling in rippled dunes in the desert. The concept of self-organization is an important hallmark of living systems, as the philosopher I. Kant described in 1790 in his definition of life: a "self-organized, self-reproducing" process, where the functions of the complete organism emerge from the properties of the parts and the whole [3].

A feature of self-organized systems is the occurrence of sudden transitions from one pattern to another as a consequence of even small changes in a parameter of the system around a critical value [2]. This property is marvelously in accordance with the concept of life: the appearance of a differentiated ensemble from uniformly distributed, identical cells is, in effect, a great example of self-organization. This fascinating morphogenesis phenomenon is what attracted Alan Turing's brilliant intellect in the first place, when in 1952 he came up with "one of the most important papers in theoretical biology" [4]. In "The chemical basis of morphogenesis", Turing explains how diffusion and interactions between components called morphogens, initially homogeneously distributed, can

lead to pattern formation and embryonic development under certain theoretical conditions. However, the key "ingredients" of the process were not clear at that time. An important principle that helped to extend Turing's mathematical work was described by Gierer and Meinhard in 1972. Patterns are based on mutual interaction between two players: a short-range activator stimulates its own production (positive feedback loop) while promoting, at the same time, the production of an inhibitor (negative feedback loop), which diffuses much faster and prevents the activator's self-amplification (Fig. 1.2). In practice, while the activator self-amplifies and accumulates in patches, the inhibitor concentration increases and prevents the next patch from forming too close by. Symmetry breaks because small, local fluctuations in the concentration of components are amplified by feedback loops, and patterns emerge [5].

Although Turing's model of reaction-diffusion systems was inspired by a key biological process, Turing equations have revealed to be too simplistic to provide a full comprehension of natural systems, which are much more complex and display a wider range of nonlinear behaviors (e.g. cooperativity or ultrasensitivity) compared to simpler inorganic systems [2, 3, 6]. Therefore the astoundment for the emergence of order is still present, as scientists are craving to find an explanation to the origin of forms in nature. One way to try to solve this riddle is to investigate a relatively simple self-organized molecular system. The Min system is one of these, representing a paradigm for protein pattern formation.

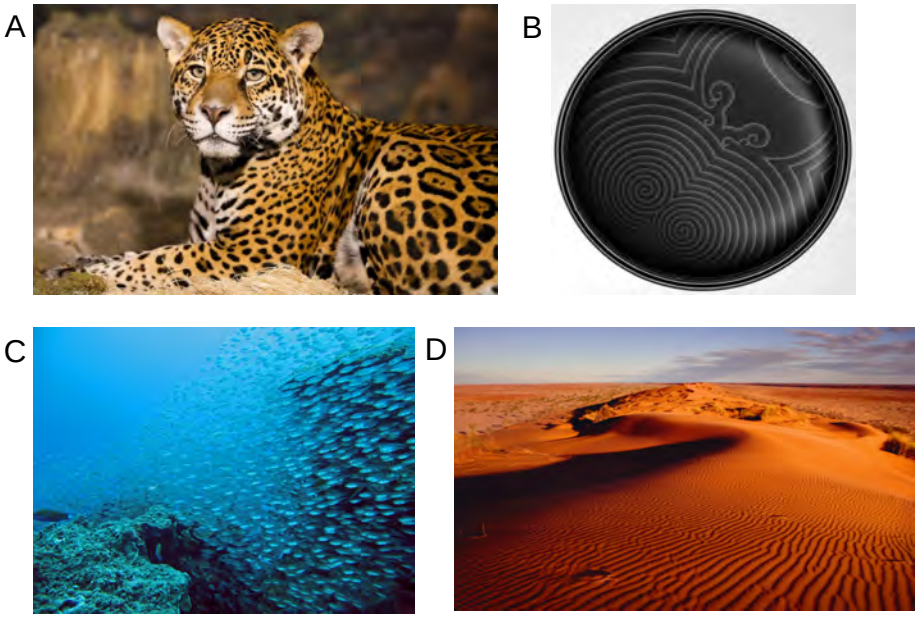

FIGURE 1.1: Self-organization occurs on different scales in various systems. A) Pigmented skin of a leopard [7], B) Spiral pattern of the Belousoz-Zhabotinsky chemical reaction in a Petri dish [8], C) School of fish [9], D) Rippled dunes of sand in the desert [10].

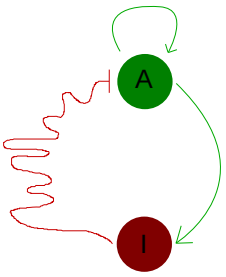

FIGURE 1.2: Schematic of the activator-inhibitor network. A short-range activator (green) stimulates its own production and promotes, at the same time, the production of an inhibitor (green arrows). The inhibitor (red) inhibits the activator's self-amplification via long-range interactions (red rugged path).

1.2 The Min system

The Min system regulates cell division in *E. coli* [11]. The molecular machinery orchestrating division is called the "divisome", and it is composed of ancestral homologues of eukaryotic cytoskeletal proteins (see Ref. [12] for review). FtsZ is a tubulin homolog [13] that assembles into the so-called "Z-ring" and determines the division plane [14]. FtsA and ZipA assist in the formation of the Z-ring by anchoring FtsZ to the membrane [15], and another set of downstream proteins is recruited later to form the complete, functional divisome [16]. Precise localization of the future division site is critical for symmetrical binary fission. Correct assembly of the Z-ring at midcell is therefore regulated by two complementary mechanisms: nucleoid occlusion (NO), a partially-understood mechanism preventing Z-ring formation near the nucleoid during chromosome segregation [17], and the Min system.

The Min system inhibits Z-ring assembly everywhere but in the middle of the cell [18] (Fig. 1.3). The system is composed of three proteins encoded by the *minB* operon. MinC directly inhibits Z-ring formation by interfering with FtsZ polymerization [19]. Dynamic localization of MinC is mediated through the spatiotemporal oscillations of the membrane-binding ATPase MinD and its activator MinE from cell pole to cell pole [18]. By oscillating together with MinD and MinE, a time-averaged concentration gradient of MinD and MinC with minimum at midcell is established: here FtsZ assembly is not inhibited and the division plane can thus be established (see Ref. [20] for review).

Min oscillations arise from repetitive cycling of the proteins between the plasma membrane and the cytosol (Fig. 1.3). MinD dimerizes upon ATP binding and interacts with the membrane [21–23]. MinE is recruited to MinD and stimulates ATP hydrolysis by MinD, triggering MinD release from the membrane and its return to the monomeric state [21, 24]. ATP hydrolysis by MinD thus contributes the energy for the oscillatory

dynamics. Importantly, the FtsZ inhibitor MinC does not play any role in the oscillations but only acts as a passenger; thus, only MinD and MinE are responsible for the dynamics [18, 25].

The oscillations of Min proteins is what makes the system of particular interest. Together with the Kai system (the circadian clock from cyanobacteria) [26], the Min system exemplifies a relatively simple biological oscillator only based on biochemical reactions between a few proteins [27]. Oscillators are probably the simplest case of complex dynamics in biology [28]. Min protein self-organization into regular, oscillatory patterns thus represents a suitable system to investigate biochemical pattern formation.

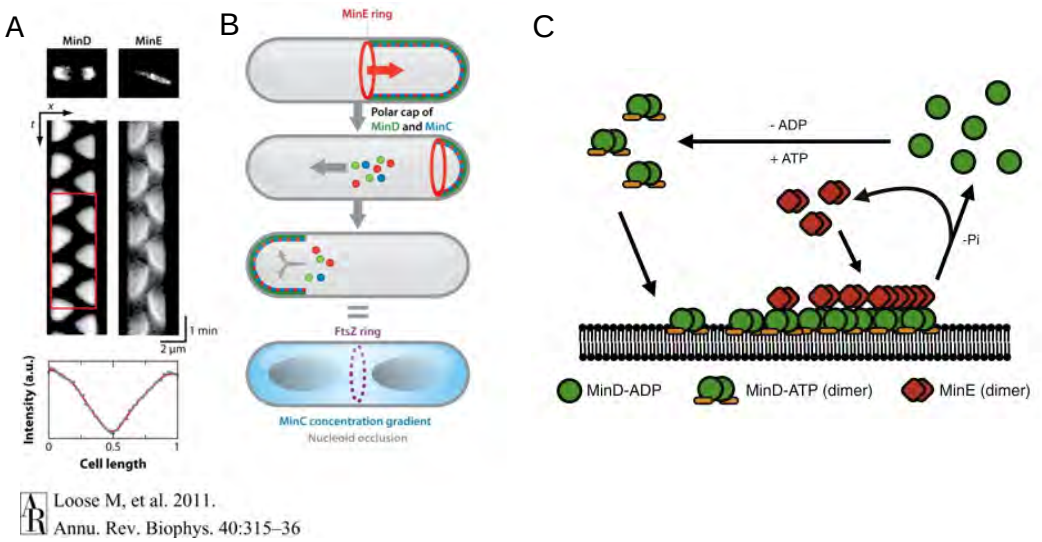

FIGURE 1.3: Min protein oscillations. "A) Top: Micrographs of GFP-MinD and MinE-GFP in vivo. Middle: Kymograph of pole-to-pole oscillations of MinD and MinE in cells of normal length (shorter than 5 μm). Bottom: Time-averaged intensity profile along the red rectangle shown in the kymograph. B) Illustration of Min protein dynamics in *Escherichia coli*: MinD-ATP (green) binds to the membrane and recruits MinC (blue). MinE (red) displaces MinC and then stimulates MinD ATPase activity, causing the release of proteins from the membrane. All three proteins diffuse through the cytoplasm and, after nucleotide exchange by MinD, [the membrane binding-unbinding is repeated]. Bottom: Illustration of the inhibitory gradient of MinC and nucleoid occlusion (gray ellipsoids), which together restrict FtsZ polymerization (purple) to the center of the cell" (adapted from Loose, M., *et al.* (2011) [27]). C) Biochemical reactions underlying the oscillations. MinD dimerizes upon ATP binding and interacts with the membrane. MinE interacts with MinD and stimulates MinD's ATP hydrolysis, triggering MinD detachment from the membrane and its return to the monomeric state (adapted from Loose, M., and Schwille, P. (2009) [29]).

1.3 *In vitro* self-organization of Min proteins

With the advent of high-throughput biology it has become more and more clear how cells can be seen as composed of a multitude of functional modules. One definition of module describes it as an autonomous entity whose function cannot be predicted by the properties of its single components [30]. In this view, the Min system can be seen like a module. One way to study a module is to reconstitute it *in vitro* from its elements.
In 2008 it was shown that Min proteins can self-organize *in vitro* on supported lipid membranes [31] (Fig. 1.4). Purified MinD, MinE, ATP, and a supported lipid bilayer (SLB) mimicking the *E. coli* inner cell membrane are sufficient for Min proteins to self-organize into planar surface waves, as previously predicted by theoretical models [32]. The patterns are stable for several hours and show features similar to the *in vivo* patterns: the temporal period is comparable to the MinD oscillatory dynamics in the cell (around 1-2 min) and is influenced by the MinE/MinD concentration ratio [31, 33]. Moreover, the MinE concentration is maximal at the rear of the wave, behind the maximum of MinD concentration; this resembles the E-ring formation *in vivo* [31, 34]. Lastly, the properties of the waves are essentially the same with and without MinC; this confirms that the protein is merely a passenger of the patterns formed by MinD and MinE and not detrimental for pattern formation [18, 27].

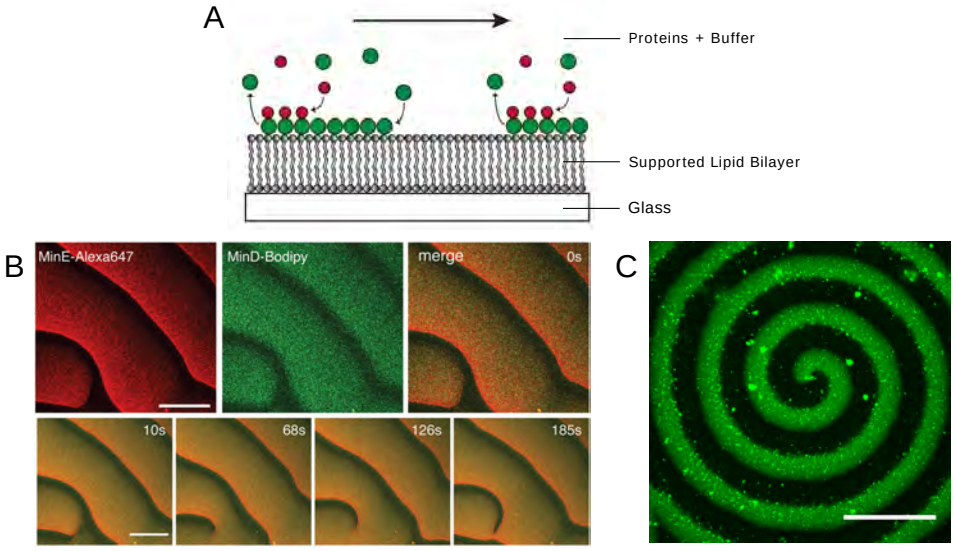

FIGURE 1.4: Min proteins self-organize into surface waves *in vitro*. A) Schematic of the *in vitro* setup. Min proteins are incubated on a supported lipid bilayer and show oscillatory dynamics. The arrow indicates the direction of propagation of the dynamics (image provided by Simon Kretschmer). B) When incubated on a supported lipid bilayer, MinE and MinD form spatially periodic bands that move in one direction. The localization of the proteins within one band resembles the in vivo situation, forming a sharp line at the trailing edge, the MinE ring (taken from Loose, M., and Schwille, P. (2009) [29]). C) Spiral pattern of eGFP-MinD (1 μM) incubated on a supported lipid bilayer in the presence of MinE (1 μM) and ATP (2.5 mM). Scale bar: 50 μm.

These findings show that a small self-organizing biochemical system can be rebuilt in a simple setup: this represents suitable conditions to investigate pattern formation at the biomolecular level. Different strategies can be adopted and several parameters can be tuned for this purpose. For example, the effect of physicochemical factors such as membrane lipid composition and salt concentration have recently been investigated and shown to have an effect on the dynamics [35, 36]. Moreover, by incubating Min proteins in microfabricated polydimethylsiloxane (PDMS) compartments of different sizes and geometries, it has been shown that geometrical cues can modulate Min protein self-organization [36, 37].

Another important question is how the biochemical features of Min proteins influence pattern formation. Studying the *in vitro* self-organization of Min protein mutants may help in identifying parameters important for the dynamics, such as binding and reaction rates. Results from such experiments can then be implemented in theoretical approaches to help obtain a rigorous model of the system.

1.4 MinD, a peripheral membrane-binding ATPase

MinD is a peripheral membrane ATPase and belongs to the family of Walker A cytoskeletal ATPases (WACA proteins). This can be considered as a family of cytoskeletal elements that have no known counterpart to eukaryotic cytoskeletal proteins [38]. Most bacteria encode one or more members of the family, which includes MinD, ParA (involved in plasmid segregation), Soj (chromosome segregation), and NifH (the Fe protein in the nitrogenase complex). A unique feature of WACA proteins is the presence of a deviant Walker A motif, which contains two lysines: one classical lysine at the carboxyl end of the motif and a second "signature" lysine at the beginning (Table 1.1) [39].

TABLE 1.1: Walker A motifs. The signature lysine in the deviant Walker A motif is shown in red, the lysine found in all Walker A motifs is colored in blue.

Classic	G	X	X	G	X	G	K	(T/S)
Deviant	X	K	G	G	X	X	K	(T/S)
MinD	G_{10}	K	G	G	V	G	K	T_{17}

WACA family members show a high conservation of primary sequence and three-dimensional structure. Furthermore, all of them undergo ATP-dependent dimerization and their ATPase activity is substantially enhanced when an "activation" protein is present [38]. In the case of MinD, its ATPase activity is stimulated around 10-fold by MinE in the presence of phospholipid vesicles [24].

MinD shows a unique feature among the WACA family members: the presence of a

membrane targeting sequence (MTS) at the C-terminus of the protein, conserved across bacteria, archaea, and chloroplasts [40]. This 8- to 12-residue sequence motif mediates membrane localization of the protein. The MTS forms an amphipathic helix that binds preferentially to anionic phospholipids [35, 41]; several hydrophobic residues in the MTS insert into the bilayer and are necessary to mediate protein-lipid interaction [42, 43]. Notably, membrane binding of *E. coli* MinD is ATP-dependent: ATP binding triggers MinD dimerization, whereby MinD acquires sufficient affinity to the membrane [23] (Fig. 1.5). In fact, one MTS from *E. coli* MinD is insufficient to promote membrane binding of GFP *in vivo* unless another MTS is present in local proximity [22]. Interestingly, MinD from gram-positive bacteria may not have to oligomerize to interact with the membrane: this is consistent with the result that one *B. subtilis* MTS is sufficient to promote protein-membrane interaction *in vivo* [22]. It has also been shown that ATP-bound MinD binds lipid vesicles in a self-enhancing fashion [21]. An accepted mechanistic model suggests MinD's cooperative assembly on membrane [22]. Detachment from the membrane is finally triggered by MinE, which stimulates MinD's ATP hydrolysis: MinD goes back to the monomeric state and dissociates from the bilayer.
It is clear that MinD membrane-binding and MinE-stimulated ATP hydrolysis represent key determinants of Min protein oscillations. One possible approach to study their effect on pattern formation is to interfere sistematically with these two processes.

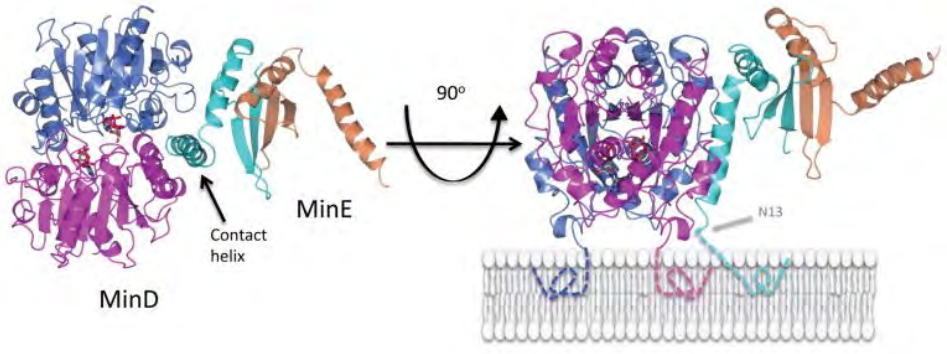

FIGURE 1.5: Structure of the MinD-MinE complex. In the orientation on the left the membrane-binding surface of MinD is beneath MinD. On the right the MinD-MinE complex is rotated 90˚so the orientation with respect to the membrane can be observed. The MTSs of MinD and MinE are depicted with dotted lines (adapted from Park, KT, *et al.* (2011) [44]).

1.5 Engineering MinD

As mentioned previously, biochemically engineering Min proteins and analyzing the effects on pattern formation represents a valuable approach to study the dynamics. In

my work I aimed at characterizing variations in *in vitro* pattern formation by varying MinD's membrane affinity and enzymatic activity. For this purpose, I analyzed various MinD protein mutants formerly reported in the literature.

In 2003, Zhou H., *et al.* showed that membrane binding by MinD involves insertion of the hydrophobic residues within the MTS into the lipid bilayer [43]. Each of the four hydrophobic residues was replaced either with tryptophan or a charged residue. Introduction of a negatively charged amino acid, as in the case of MinD L267E, decreased membrane binding of MinD and its capacity to activate MinC in *E. coli*. MinD L267E had also been previously shown to display cytoplasmic localization [40]. These findings together underlined that membrane binding of MinD L267E was strongly compromised. On the contrary, mutants with tryptophan substitutions (such as MinD L267W) retained the ability to bind to the membrane and activate MinC; however, ability of membrane binding and stimulated ATPase activity were in some cases suggested to be less efficient than those of MinD wild type (WT) [43]. In 2002, a mutant with an amino acid insertion mimicking *B. subtilis* MTS (MinD Ins3) was shown to exhibit a distinct peripheral localization pattern *in vivo* indistinguishable from that of MinD WT [40]. *B. subtilis* MinD contains a three-amino acid insertion (AKI) in the MTS compared with *E. coli* MinD that occurs between residues corresponding to L-264 and K-265 of the *E. coli* sequence (Table 1.2). Since one single *B. subtilis* MTS is known to be sufficient to promote membrane binding of GFP (in contrast to the *E. coli* MTS) [22], it is possible that MinD Ins3 shows a stronger membrane binding capacity with respect to MinD WT. However, further analyses of membrane affinity or oscillatory behavior were not performed by Szeto, J., *et al.* (2002).

TABLE 1.2: MinD putative MTS. The *B. subtilis* MinD MTS contains a three-amino acid insertion compared to the *E. coli* MinD MTS. The three amino acids are highlighted in blue.

Escherichia coli	K	G	F	L_{264}	-	-	-	K_{265}	R	L	F
Bacillus subtilis	K	G	M	M	A	K	I	K	S	F	F

The deviant Walker A motif is responsible for ATP binding, and mutations within this region involving residues like K16 or K11 (signature lysine) have been shown to disrupt MinD's ATPase activity, protein dimerization, and association with membranes [43–46]. However, several other residues outside of the deviant Walker A motif have been suggested to play a role in the regulation of MinD's ATPase activity. Szeto, J., *et al.* (2004) analyzed the role of mutations in the extreme N-terminus of *Neisseria gonorrhoeae* MinD. Different mutants, including $MinD_{Ng}$ K3E, I4Q, and a two-amino acid deletion mutant at the N-terminus ($MinD_{Ng}$ 3aaNT), were shown to be affected in dynamic localization, protein-protein interaction, and enzymatic activity, although

none of these functions was totally abolished. These observations were in contrast to the K16Q phenotype, where MinD movement, membrane localization, and ATPase activity are completely abrogated. From these findings it was suggested that the extreme N-terminus of MinD may be involved in regulating the intrinsic ATPase activity [47].
This list of evidence provided me with two separate groups of mutants I could test *in vitro* to investigate Min protein dynamics. MinD L267E, L267W, and Ins3 were good candidates to test the effect of altered MinD membrane affinity on pattern formation, since their membrane affinity was suggested to be negligible, weaker, and stronger (respectively) compared to MinD WT. Moreover, I selected MinD K3E, I4Q, and 3aaNT to test how modulations in the ATPase rate affect pattern formation.

Chapter 2

Material and Methods

2.1 Constructs

2.1.1 Plasmids

All MinD mutants were cloned using a site-directed mutagenesis approach. Two different plasmid backbones were used as DNA templates: pET28a-eGFP-MinD (length 6880 bp) and pET28a-MinD-MinE (length 6436 bp) (Fig. 2.1). The former was used for cloning all eGFP-MinD mutants, the latter for the untagged versions. Both plasmids were generated previously in the Schwille lab. They contain a T7 promoter, a kanamycin resistance cassette, and C- and N-terminal His-tags. In pET28a-eGFP-MinD, at the N-terminus of $MinD_{2\text{-}270}$ the protein is fused to eGFP via a 6 bp-linker (CTTAAG). eGFP carries a His-tag at the N-terminus. In pET28a-MinD-MinE, MinD and MinE ORFs are present, but only MinD carries a His-tag at the N-terminus. Presence of both sequences decreases plasmid-derived toxicity in living cells.

2.1.2 Cloning

Primers were designed using the OligoAnalyzer tool by Life Technologies^{TM}. For a complete list of primers, see Appendix A.
MinD L267E, eGFP-MinD L267E, MinD L267W, MinD R3E, MinD I4Q, eGFP-MinD I4Q, MinD 3aaNT, eGFP-MinD 3aaNT were cloned using the GeneArt® Site-Directed Mutagenesis PLUS Kit (Life Technologies^{TM}). The protocol for *in vitro* one site-directed mutagenesis was followed.
eGFP-MinD L267W, MinD Ins3, eGFP-MinD Ins3 were cloned using a temperature gradient site-directed mutagenesis approach. All mutated plasmids were verified by

sequencing (Max-Planck-Institut für Biochemie - Martinsried - DNA sequencing facility). For a more detailed version of the mutagenesis protocols, see Appendix B.

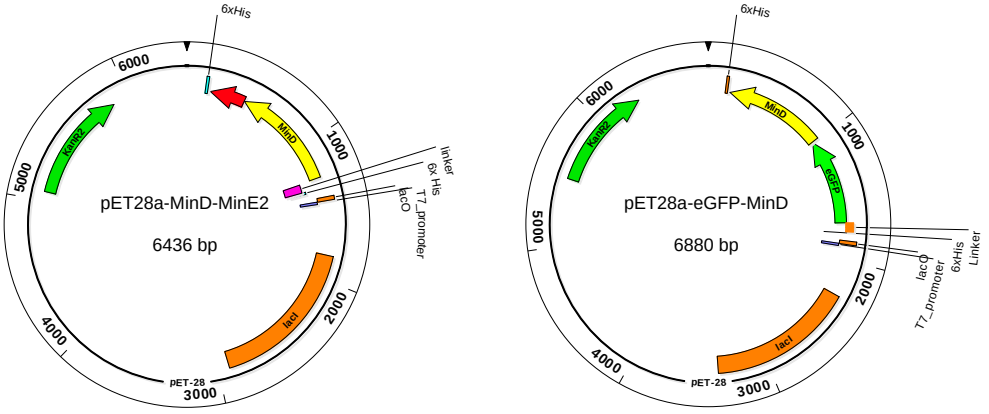

FIGURE 2.1: Plasmid maps. Schematic of pET28a-MinD-MinE (left) and pET28a-eGFP-MinD (right). The main features are highlighted: T7 promoter, lacI, His-tags, kanamycin resistance cassette, ORFs of the genes of interest.

2.1.3 Glycerol stocks of cultures with verified plasmids

One clone for each construct was picked among the verified clones. 1 μL plasmid DNA was transferred into one 50-μL vial of electrocompetent cells (BL21(DE3) or XL1-Blue (Max-Planck-Institut für Biochemie - Martinsried)). Cells were electroporated for 5-6 ms at 2500 V. Then 500 μL SOC medium were added to the electroporated cell suspension and the vials were incubated for 30-60 min at 37 °C at 600 rpm. 150 μL XL1-Blue cell suspensions were plated on LB Kan agar plates. 100 μL BL21(DE3) cell suspensions were added to 5 mL LB Kan medium and grown O/N at 37 °C at 220 rpm. Then 200 μL O/N culture was transferred into 5 mL fresh LB Kan medium and grown for 4 h at 37 °C at 220 rpm. 500 μL of 50 % sterile glycerol was added to the cell suspension at a ratio of 1:1 and glycerol stocks were stored at -80 °C.

2.2 Protein expression and purification

2.2.1 Protein expression

For expression of untagged MinD mutants, a sample of culture from the corresponding glycerol stock was grown in LB Kan O/N at 37 °C at 220 rpm. 5 mL of the O/N culture was diluted in 400-500 mL of fresh Terrific Broth (TB) Kan medium and growth was continued at 37 °C at 220 rpm to an optical density at 600 nm (OD600) of 0.7. To

induce overproduction of the protein of interest, Isopropyl β-D-1-thiogalactopyranoside (IPTG) was added to 1 mM final concentration and growth was continued for 3-4 h at 37 °C at 220 rpm. Cells were centrifuged for 10 min in a JA-10 rotor (Beckman Coulter®) at 4500 g and 4 °C using a Beckman Coulter®Avanti® J-26XP centrifuge. The supernatant was discarded and the pellet resuspended in fresh LB Kan medium. Cells were transferred to 50-mL falcon tubes and again centrifuged for 10 min at 4500 g and 4 °C. The supernatant was discarded and the pellet stored at -80 °C.
MinE (Simon Kretschmer's glycerol stock) was expressed using the same protocol as for MinD untagged mutants.

For expression of eGFP-MinD mutants, a sample of culture from the corresponding glycerol stock was grown in TB Kan medium for 5-6 h at 37 °C at 220 rpm. 5 mL of the O/N culture was diluted in 400-500 mL of fresh TB Kan medium and growth was continued at 37 °C at 220 rpm to an OD600 of 0.7. IPTG was added to 1 mM final concentration to induce protein expression and growth was continued O/N at 16 °C at 220 rpm. Then cells were harvested as described above for the untagged MinD proteins.

2.2.2 Protein purification

Pellets of cells with expressed MinD and eGFP-MinD mutants were resuspended in lysis buffer (50 mM Tris pH 8.0, 300 mM NaCl, 10 mM Imidazole, 10 mM β-mercaptoethanol, EDTA-free Protease Inhibitor (Roche), 0.2 mM ADP pH 7.5). Cell suspensions were lysed by four passages through an EmulsiFlex-C3 homogenizer (Avestin). Lysates were then centrifuged for 45 min in a JA-25.50 rotor (Beckman Coulter®) at 25000 g and 4 °C in a Beckman Coulter® Avanti® J-26XP centrifuge. The supernatant was loaded onto a NiNTA-superflow column (QIAGEN) and incubated for 1 h at 4 °C while shaking. The column was washed 3 times with lysis buffer (50 mM Tris pH 8.0, 300 mM NaCl, 10 mM Imidazole, 10 mM β-mercaptoethanol, EDTA-free Protease Inhibitor (Roche), 0.2 mM ADP pH 7.5) and 3 times with wash buffer (50 mM Tris pH 8.0, 300 mM NaCl, 20 mM Imidazole, 10 mM β-mercaptoethanol, 10 % glycerol, EDTA-free Protease Inhibitor (Roche)). Protein was eluted with elution buffer (50 mM Tris pH 8.0, 300 mM NaCl, 250 mM Imidazole, 10 mM β-mercaptoethanol, 10 % glycerol, EDTA-free Protease Inhibitor (Roche)). Peak MinD fractions were pooled and the elution buffer was exchanged to storage buffer (50 mM HEPES pH 7.25, 150 mM KCl, 10 % glycerol, 0.1 mM EDTA, 0.2 mM ADP pH 7.5, 0.4 mM TCEP) using Econo-Pac® 10DG desalting columns (BioRad). Proteins were aliquoted and stored at -80 °C. Protein concentration was assessed by Bradford assay. For the protocol of the Bradford assay and the determined protein concentrations, see Appendix C. Protein purity was assessed with Sodium

Dodecyl Sulfate Polyacrylamide Gel Electrophoresis (SDS-PAGE) and gels were stained with Coomassie Blue after electrophoresis. For Coomassie stained polyacrylamide gels of purification fractions, see Appendix D.

MinE was purified using the same protocol as for MinD mutants. Notably, lysis buffer and elution buffer for MinE purification did not need to contain ADP. At high concentrations, MinE is prone to aggregation; therefore, before proceeding with aliquotation the sample was centrifuged for 30 min with a MLA-130 rotor (Beckman Coulter®) at 50000 g and 4 °C using a Beckman Coulter® Optima™ MAX-XP Ultracentrifuge to remove aggregates.

2.3 Preparation of lipid membranes

Lipid bilayers on solid supports are a widely used model system for biological membranes. Mobility of individual lipids is preserved as in biological contexts, and a membrane confined to the surface of a glass coverslip represents a suitable substrate to image lipid and/or protein dynamics by fluorescent microscopy.

2.3.1 Preparation of Small Unilamellar Vesicles (SUVs)

64 μL of *E. coli* polar lipids (Avanti® Polar Lipids) dissolved in chloroform were transferred to a glass vial and the solvent was evaporated under a gentle stream of nitrogen. Any residual solvent was further removed by drying the lipid film in vacuum for 30 min. Lipids were rehydrated in 400 μL membrane buffer (25 mM Tris-HCl pH 7.5, 150 mM KCl) to a lipid concentration of 4 mg/mL and incubated for 1 h at 37 °C. The lipid film was then completely resuspended by vortexing vigorously during and at the end of the incubation time: this process facilitates the formation of multilamellar vesicles of different sizes. The sample was then placed in a bath sonicator and sonicated for 10-15 min: during this time the size of the vesicles decreases and SUVs form. SUVs were stored at -20 °C as 20 μL-aliquots.
For some experiments SUVs labeled with a fluorescent dye were needed. In these cases, 0.1 % DiD (Invitrogen) was added to *E. coli* polar lipids in the glass vial before proceeding with evaporation of the solvent.

2.3.2 Formation of Supported Lipid Bilayers (SLBs)

SLBs used for self-organization assays were prepared inside reaction chambers. The reaction chamber was prepared by attaching a plastic ring on a glass coverslip using

ultraviolet (UV) glue (Norland Optical Adhesive 68). A suspension of SUVs was diluted with 130 μL membrane buffer (25 mM Tris-HCl pH 7.5, 150 mM KCl) to 0.5 mg/mL and 75 μL were added to the reaction chamber. The sample was incubated for 20 min at 37 °C: during this time, vesicles adsorbed to the surface, ruptured and fused to form a flat bilayer (Fig. 2.2). Adding 3 μL of $CaCl_2$ to a final concentration of 3 mM, supported vesicle rupture and formation of the bilayer. The sample was finally washed with 2 mL of membrane buffer pre-warmed at 37 °C. Membrane buffer was exchanged with reaction buffer (25 mM Tris-HCl pH 7.5, 150 mM KCl, 5 mM $MgCl_2$) before proceeding with the assay.

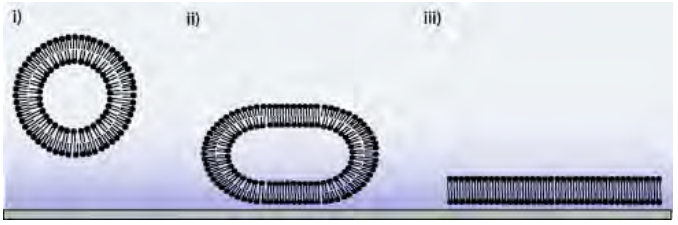

FIGURE 2.2: Preparation of supported lipid bilayers. Vesicles adsorb to the support (i), are deformed (ii) and rupture spontaneously (iii) (taken from Loose, M., and Schwille, P. (2009) [29]).

2.4 Functional assays

2.4.1 Cosedimentation assay

The ability of MinD mutants to bind membranes was qualitatively assessed via a cosedimentation assay. The strategy was adapted from Loose M., and Mitchison TJ., (2014). 5 μM purified protein was added to a suspension of 0.5 mg/mL sonicated SUVs in reaction buffer (25 mM Tris-HCl pH 7.5, 150 mM KCl, 5 mM $MgCl_2$) to a final 50 μL volume. The assay was started by adding 1 mM adenosine triphosphate (ATP) and incubated for 15 min at RT. Vesicles were sedimented by centrifuging for 10 min in a TLA-100 rotor (Beckman Coulter®) at 25000 rpm at RT using a Beckman Coulter® Optima™ MAX-XP Ultracentrifuge. The supernatant was carefully separated from the pellet fraction and collected. The pellet was resuspended in reaction buffer to the original volume. The amount of protein in the pellet and supernatant fractions was estimated by SDS-PAGE. Gels were stained with Coomassie Blue after electrophoresis. Controls without vesicles were run to show that the pelleted amount of protein was due to membrane interaction.

2.4.2 Z-scans of proteins on SLBs

Affinity of MinD to membranes was also assessed using confocal microscopy. 0.5 μM MinD mutants (70 % untagged protein, 30 % eGFP-tagged protein) were added to the reaction buffer in the reaction chamber (Fig. 2.4). 2.5 mM ATP was subsequently added and the sample was incubated for 30-60 min at RT before imaging. The final volume of the assay was 200 μL. The purpose was to check for localization of proteins on the membrane: DiD-labeled SUVs were used to prepare SLBs, in order to check for eGFP/DiD signal colocalization. The chamber was closed with a lid of an Eppendorf tube during observation. Confocal imaging was performed using a Zeiss laser scanning microscope (LSM) 780 (Zeiss) with a Zeiss C-Apochromat 40x, NA=0.75 water immersion objective. Laser power was adjusted depending on the available signal intensities, therefore fluorescence intensities were not directly comparable between experiments. eGFP was excited with an Argon laser of 488 nm wavelength; the excitation wavelength for DiD was 647 nm. The fluorescence signal was detected with a photomultiplier (PMT). A Z-stack of the sample ranging from below to above the membrane was recorded. Z-stacks were analysed with the image processing software Fiji Is Just Image J (Fiji).

2.4.3 ATPase activity assay

ATPase activity of MinD mutants was tested in the presence of MinE and phospholipids. To quantify ATP hydrolysis a coupled enzymatic assay was used (see Fig. 2.3 for a schematic of the reactions). 4 μM MinD and 4 μM MinE were added to a premix of 0.2 mg/mL sonicated SUVs, 0.5 mM reduced nicotinamide adenine dinucleotide (NADH), 2 mM phosphoenolpyruvic acid (PEP), 30/20 U/mL pyruvate kinase/lactate dehydrogenase (PYK/LDH) in reaction buffer to a final volume of 150 μL (all reagents from Sigma-Aldrich). The reaction was incubated for 5 min at RT to remove possible ADP contaminants. 1 mM ATP was added and absorbance at 340 nm was immediately followed for 30 min with a JAS.C.O® V-650 spectrophotometer.

NADH has an absorption maximum at 340 nm and an extinction coefficient of 6220 $M^{-1}cm^{-1}$. Since consumption of 1 mol NADH is stoichiometrically equivalent to the consumption of 1 mol ATP, the ATPase rate can be calculated from the slope of the resulting curve and the extinction coefficient of NADH:

$$ATPase\ activity\ (\tfrac{nmol}{mg*min}) = \frac{slope}{\varepsilon_{NADH}(nM^{-1}*cm^{-1})*pathlength(cm)*MW(g/mol)*prot.conc.(M)}$$

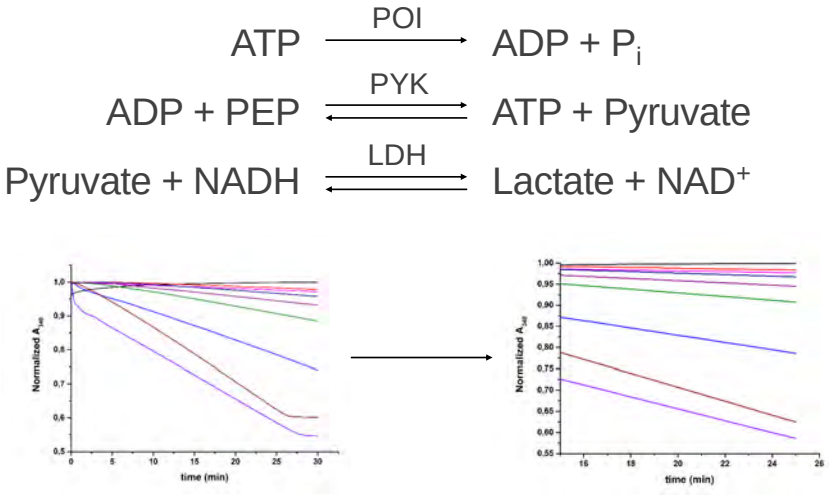

FIGURE 2.3: Principle of the coupled enzymatic ATPase assay. Three reactions occur (top): ATP is hydrolyzed to ADP and inorganic phosphate (Pi) by the protein of interest (POI); ADP reacts with PEP to ATP and pyruvate catalyzed by pyruvate kinase (PYK); lactate dehydrogenase (LDH) catalyzes the oxidation of NADH to NAD^+ while converting pyruvate to lactate. Decay of NADH absorption at 340 nm is followed over time (bottom left). The linear part of the resulting curve is used to calculate the enzymatic activity of the protein of interest (bottom right).

2.4.4 Self-organization assay

Self-organization of Min proteins was assessed at different absolute concentrations of MinD and MinE and also at different concentration ratios of MinD/MinE. MinD (70 % untagged protein, 30 % eGFP-tagged protein) and MinE were added to the reaction buffer in the reaction chamber (Fig. 2.4). 2.5 mM ATP was subsequently added to a final volume of 200 μL. Samples were usually incubated for 30-60 min at RT before imaging. The chamber was closed with a lid of an Eppendorf tube during observation. Confocal imaging was performed using a Zeiss LSM 780 microscope with a Zeiss C-Apochromat 40x, NA=0.75 water immersion objective. In most of experiments, the laser power was adjusted depending on the available signal intensities. Therefore, fluorescence intensities were not directly comparable between experiments. eGFP was excited with a 488 nm wavelength. The fluorescence signal was detected with a PMT. Images were analysed with the image processing software Fiji.

Every experiment with MinD mutants was compared to a MinD WT sample prepared fresh on the same day. Most of the experiments involved titrations of the protein in the reaction chamber. This means that the protein concentration in the chamber was progressively increased over time and imaged after 30-60 min of incubation at the new concentration at RT.

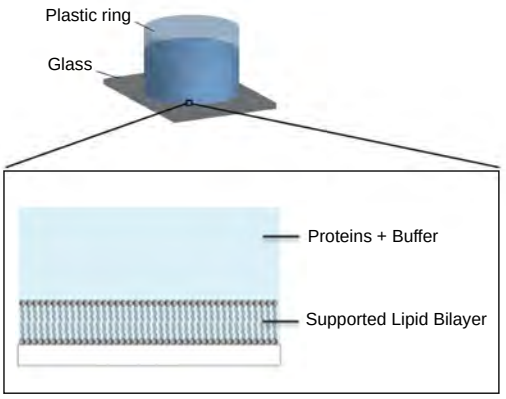

FIGURE 2.4: Experimental setup. The reaction chamber is composed of a plastic ring glued on a glass coverslip. A supported lipid bilayer is formed on the bottom of the reaction chamber and proteins and ATP are incubated in the reaction buffer on top of the membrane (image adapted from Zieske, K., *et al.* (2014) [48] and from Kretschmer, S., and Schwille, P., (2014) [49]).

Chapter 3

Results

From the literature I identified the list of *E. coli* MinD mutants I wanted to use to test Min protein self-organization. As described previously, the mutants can be subdivided into two categories according to the MinD function that was expected to be affected by the mutation (Table 3.1).

TABLE 3.1: List of MinD mutants. The MinD mutants I worked with can be subdivided into two categories depending on the protein function that was reported to be affected by the mutation: membrane binding or ATPase activity.

Membrane binding mutants	**ATPase mutants**
L267E	R3E
L267W	I4Q
Ins3	3aaNT

MinE and all the MinD mutant proteins were successfully cloned, expressed, purified, and tested for enzymatic activity and self-organization properties as described in Chapter 2. Especially for self-organization assays I needed a fluorescently-tagged version of each mutant that could be observed using Laser Scanning Confocal Microscopy. For this purpose, I cloned and purified both an untagged and an N-terminal enhanced green fluorescent protein (eGFP)-tagged version of each mutant, for a total of 11 proteins (Fig. 3.1). I encountered difficulties cloning the 12^{th} mutant and I could not complete it myself due to time constraints. The cloning of eGFP-MinD R3E was then kindly overtaken by Michaela Schaper and successfully completed.

I tested all the purified proteins at different levels using biochemical and biophysical techniques. MinD membrane binding mutants (MinD L267E, L267W, Ins3) were tested for their ability to bind to the membrane. The ATPase activity was also measured, before testing the self-organization capacity and characterizing the patterns.

Enzymatic activity of the ATPase mutants (MinD R3E, I4Q, 3aaNT) was assessed, as well as their self-organization ability.
In all the experiments, MinD WT was used as reference. MinD WT and eGFP-MinD WT proteins were purified by the Biochemistry Core Facility of the institute.

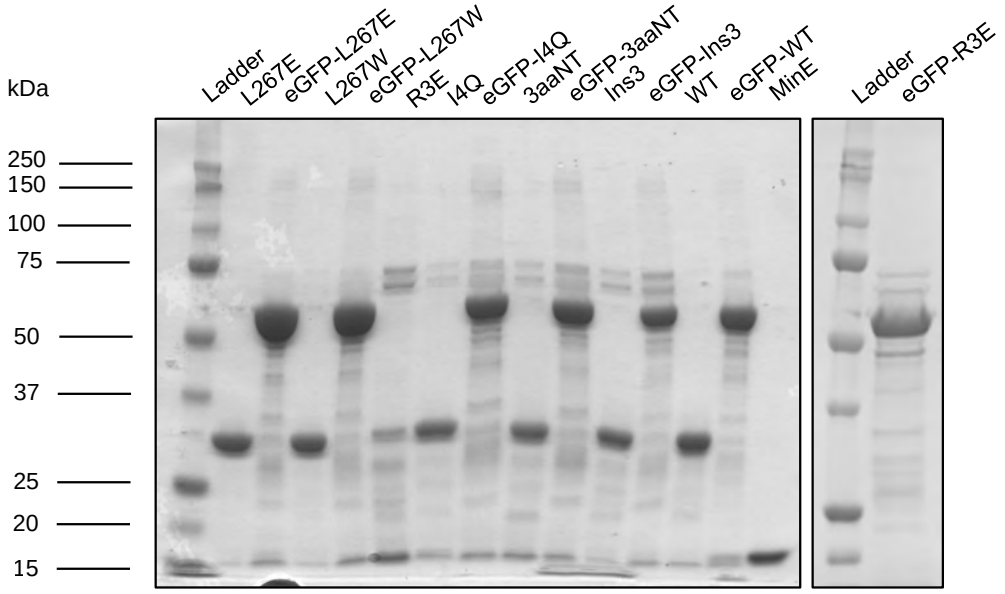

FIGURE 3.1: Coomassie Blue stained Mini-Protean TGX polyacrylamide gels 10 % (Bio-Rad) of purified MinD mutants, MinD WT, MinE. All proteins were diluted to a final concentration of 5 μM. Mass of untagged MinD proteins is around 33300 Da; mass of eGFP-tagged MinD proteins is around 60100 Da; mass of MinE is 13923.9 Da.

3.1 MinD mutants with altered membrane affinity

MinD L267E, L267W, and Ins3 carried mutations in the MTS. In previous works by Zhou, H. *et al.* (2003) and Szeto, H. *et al.* (2002), these mutants were studied *in vivo* and suggested to have different binding affinities to the membrane compared to the WT. Alterations in membrane binding were further shown to have effects on the activity of the protein [40, 43]. As a first characterization, affinity for membranes was investigated *in vitro*. Afterwards, enzymatic assays were performed to test whether mutations in the membrane-binding domain could have any effects on the ATPase activity of the protein. Ultimately, self-organization assays with different concentrations of the proteins were performed on SLBs to study how Min protein pattern formation changed upon modulating MinD membrane binding.

3.1.1 Qualitative assessment of membrane binding

Membrane affinity of MinD L267E, L267W, and Ins3 was assessed qualitatively with two *in vitro* assays: a cosedimentation assay and Z-scan confocal imaging of proteins on SLBs (methods are described in Sections 2.4.1 and 2.4.2). In all tests, MinD WT was used as reference. All experiments were run at least in triplicate.

Cosedimentation assay

In the cosedimentation assay MinD was incubated with phospholipids in the presence of ATP and the mixture was centrifuged to test whether the protein coprecipitated with lipids or stayed in the supernatant. Cosedimentation of MinD with lipid vesicles indicated membrane binding. Negative controls without lipids were run to corroborate the results.

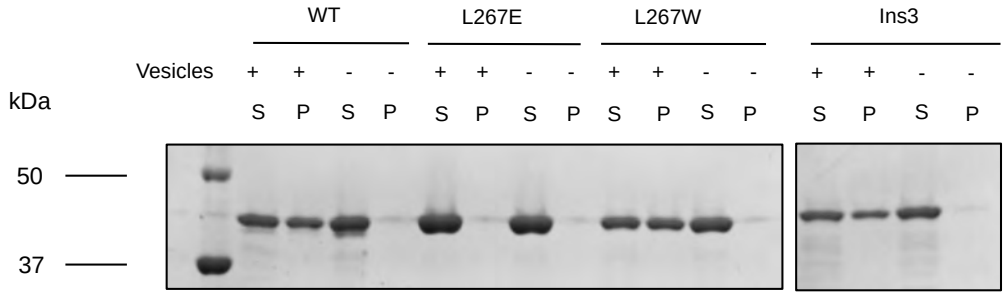

FIGURE 3.2: Cosedimentation of MinD WT and mutants with lipid vesicles. The Coomassie Blue stained Mini-Protean TGX polyacrylamide gels 10 % (Bio-Rad) show supernatant (S) and pellet (P) fractions of 5 μM MinD WT, L267E, L267W, Ins3 incubated with 0.5 mg/mL lipid vesicles in the presence of 1 mM ATP and then centrifuged at 25000 g for 10 min. Negative controls without lipid vesicles were run.

MinD WT coprecipitated with the lipid vesicles, as expected. Part of the protein was in the pellet, part in the supernatant. On the contrary, MinD L267E was all present in the supernatant: this was an indication of MinD L267E's inability to bind phospholipids. A difference in membrane binding between MinD L267W and MinD Ins3 and MinD WT was not observed with this assay. Controls without lipid vesicles did not show protein in the pellets, as expected (Fig. 3.2).

Z-scans

Confocal microscopes allow to scan samples along the vertical (Z) axis. I used Z-scans of MinD mutants incubated on SLBs in the presence of ATP to look at the colocalization of eGFP-tagged proteins and DiD-labeled lipids. Colocalization of fluorescent signals indicated presence of proteins on the membrane.

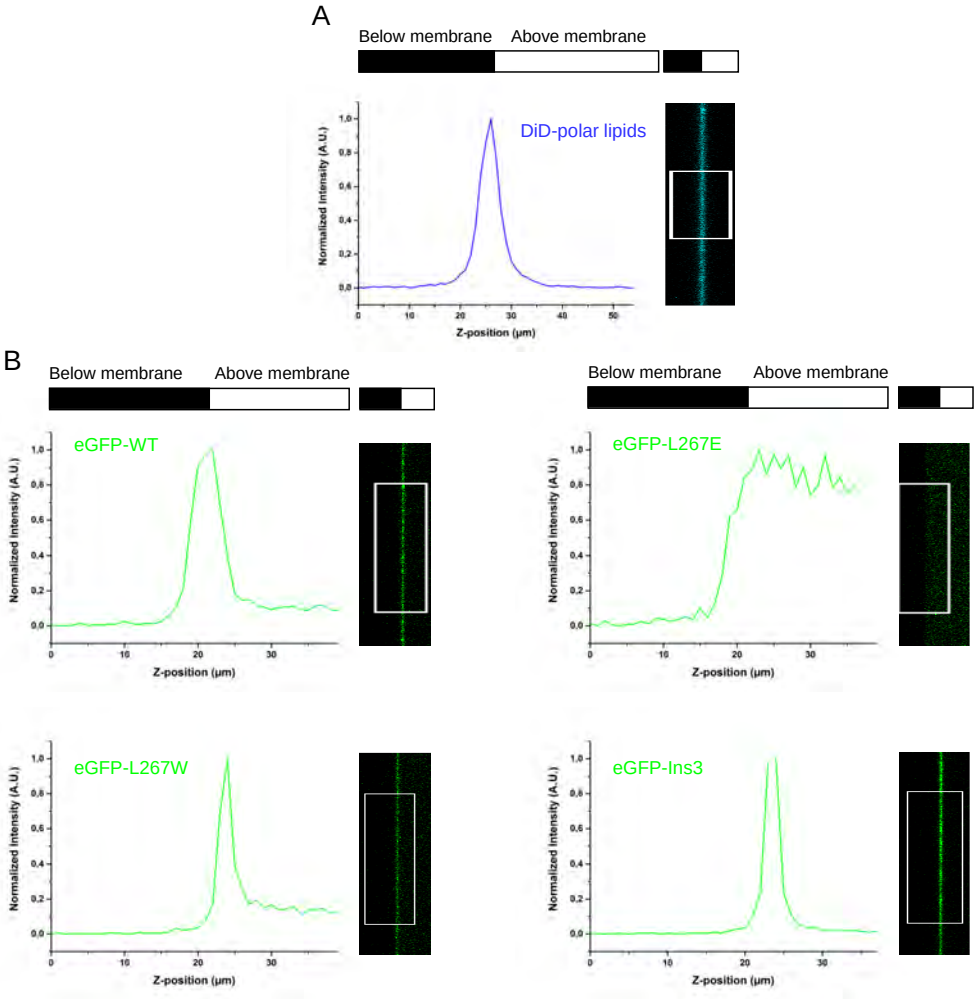

FIGURE 3.3: Z-scans of MinD WT and membrane binding mutants incubated on SLBs. A) Z-scan of DiD-labeled *E. coli* polar lipids forming the SLB (right) and corresponding profile (left) along the rectangular area shown in the Z-scan. B) Z-scans of eGFP-tagged MinD WT, L267E, L267W, Ins3 (0.15 μM) incubated on SLBs in the presence of 2.5 mM ATP (right) and corresponding profiles (left) along the rectangular areas shown in the Z-scans. 0.35 μM of corresponding untagged MinD proteins were also incubated on the membrane, to a final protein concentration of 0.5 μM.

Z-scans showed that MinD L267E was unable to bind membranes (Fig. 3.3). Fig. 3.3 shows Z-scans of proteins at a concentration of 0.5 μM incubated on SLBs. However, titrations of all proteins were performed from 0.5 μM to 3 μM but no significantly

different results were observed.
Noteworthy, MinD L267E did not bind membranes even at high concentrations of MinD (3 μM) (Fig. E.1 - Appendix E). These results suggested that L267E's inability to bind phospholipids could be attributed to the mutation and not to density or concentration factors.
A difference in membrane binding between MinD L267W and MinD Ins3 and MinD WT was not observed with this assay.

3.1.2 ATPase activity assay

ATP hydrolysis rate of MinD membrane binding mutants was measured with a coupled enzymatic assay. As explained in Section 2.4.3, ATP hydrolysis is stoichiometrically equivalent to NADH oxidation to NAD^+. By following the absorbance decay of NADH over time it was possible to calculate the rate of ATP hydrolysis by MinD. ATPase activity of MinD mutants was tested both in the presence and in the absence of MinE. Since MinE-stimulated MinD's ATP hydrolysis is known to be dependent on the presence of lipids [24], lipid vesicles were always used in the tests.

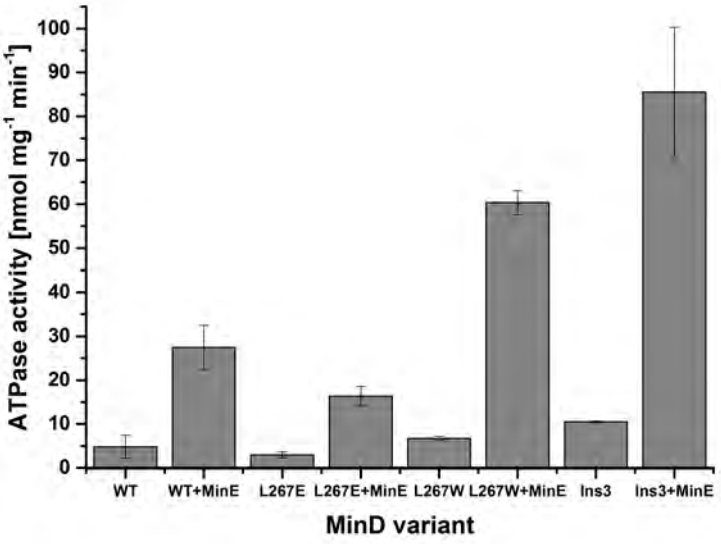

FIGURE 3.4: ATPase activity of MinD membrane-binding mutants. 4 μM MinD WT, L267E, L267W, Ins3 were incubated with and without MinE (4 μM) in the presence of phospholipid vesicles (0.2 mg/mL) in a coupled enzymatic activity assay. Error bars correspond to standard deviations resulting from three independent experiments.

MinE-stimulated ATPase activity of MinD WT was comparable to previous findings, with an average activity of 27 nmol/mg/min and about 7-fold stimulation compared to MinD's basal ATPase activity [43, 45]. Interestingly, despite negligible ability to bind membranes (see Section 3.1.1), MinD L267E showed stimulated ATPase activity.

However, MinD L267E's stimulated enzymatic activity was lower than that of MinD WT by about 60 % (Fig. 3.4). MinD L267W showed higher stimulated ATPase activity compared to MinD WT (Fig. 3.4). This result is in contrast to what was previously reported by Zhou H., *et al.*, 2003. The authors reported a lower stimulated ATPase activity of MinD L267W when compared to MinD WT, although a different ATPase assay and protein concentrations were used in these experiments [43]. MinD Ins3 had the highest stimulated and basal ATPase activities among the proteins tested, with an average 8-fold stimulation compared to basal ATPase activity (Fig. 3.4).

3.1.3 Self-organization assays

Self-organization assays were performed on SLBs as described in Section 2.4.4. In these experiments, the effect of protein concentration on pattern formation was of particular interest. The concentration of MinD mutants was titrated in the presence of an invariable concentration of MinE. In some cases, the inverse experiment was performed: MinE concentration was titrated in the presence of a constant MinD concentration. As mentioned in Section 1.3, the MinD/MinE protein concentration ratio is a major determinant of pattern formation. However, the absolute concentrations of MinD and MinE can play an important role in protein self-organization. To investigate the role of absolute concentrations more deeply, I studied the self-organization of one MinD mutant both at high (micromolar range) and low (nanomolar range) protein concentrations. In these experiments either MinD was titrated in the presence of a constant MinE concentration or the other way around.

Titrations at "high" absolute protein concentrations

Self-organization of MinD L267E, L267W, and Ins3 was assessed at the following MinD protein concentrations: 0.5, 1, 2, 3 μM. In these experiments, MinE concentration was 1 μM.

As expected from the membrane-binding assays, MinD L267E was not able to bind to the membrane at any MinD concentrations. This resulted in no pattern formation at all. MinD Ins3 appeared bound to the membrane but did not show any pattern formation at MinD concentrations of 2 and 3 μM. However, faint patterns were observed at MinD concentrations of 0.5 and 1 μM (Fig. 3.5) (this was a good reason to investigate pattern formation of MinD Ins3 further, trying low absolute concentrations of MinD and MinE - see next subsection). Interestingly, titrations of MinE from 2 to 5 μM in the presence of MinD Ins3 at 1 μM did not lead to any pattern formation: MinD Ins3 formed a carpet on the membrane with no pattern formation occurring (Fig. E.2 - Appendix E).

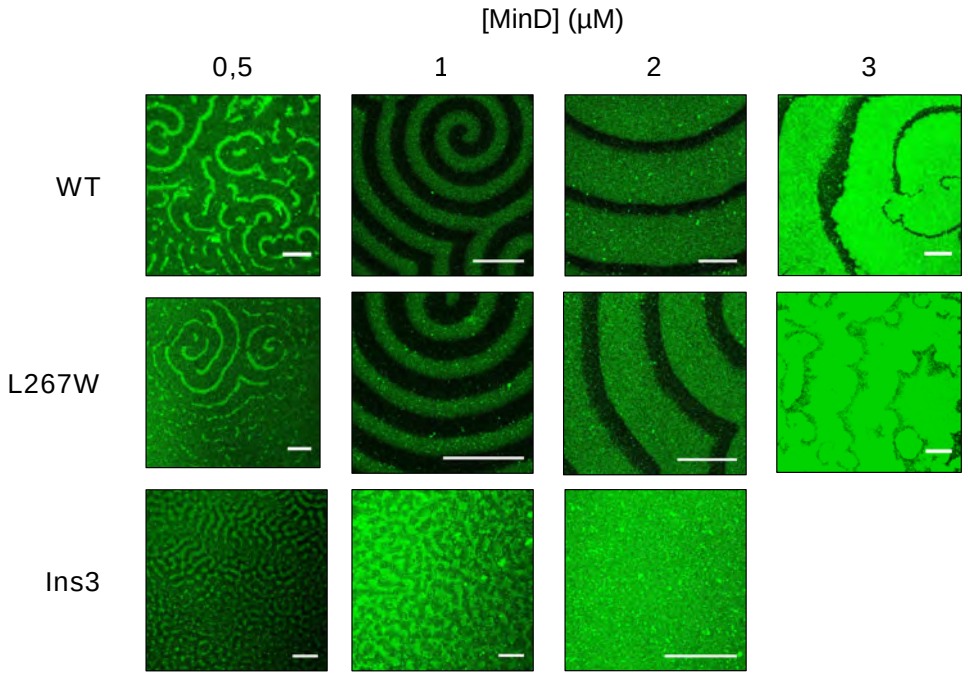

FIGURE 3.5: Self-organization of MinD membrane binding mutants at increasing MinD concentration. eGFP-MinD WT, L267W, Ins3 were observed on SLBs and displayed self-organization at certain MinD concentrations. Total MinD concentration was titrated between 0.5 and 3 μM (70 % untagged MinD, 30 % eGFP-MinD). MinE was constantly present at a concentration of 1 μM. ATP concentration was 2.5 mM. The experiments were run at least in triplicate. Scale bar: 50 μm.

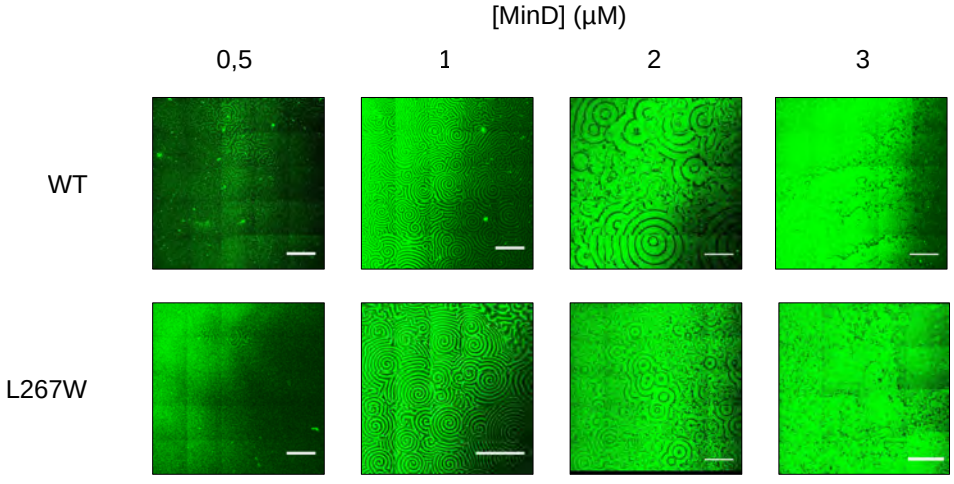

FIGURE 3.6: Self-organization of MinD WT and MinD L267W on SLBs at increasing MinD concentrations. Total MinD concentration (70 % untagged MinD, 30 % eGFP-MinD) was titrated between 0.5 and 3 μM in the presence of 1 μM MinE and 2.5 mM ATP. eGFP-tagged MinD WT and L267W showed formation of regular patterns at MinD concentrations of 1 and 2 μM. Patterns formed by MinD WT and MinD L267W look qualitatively similar. The experiments were run at least in triplicate. Scale bar: 300 μm.

MinD L267W displayed self-organization. Patterns of MinD L267W looked qualitatively similar to those formed by WT (Fig. 3.5 and 3.6). Regular travelling waves formed at MinD concentrations of 1 and 2 μM. Patterns formed also at MinD concentrations of 0.5 and 3 μM. However, patterns at MinD concentrations of 0.5 and 3 μM were irregular and not present in all replicates. Therefore, quantitative analysis of patterns was performed only on stable patterns at MinD concentrations of 1 and 2 μM (Fig. 3.7).

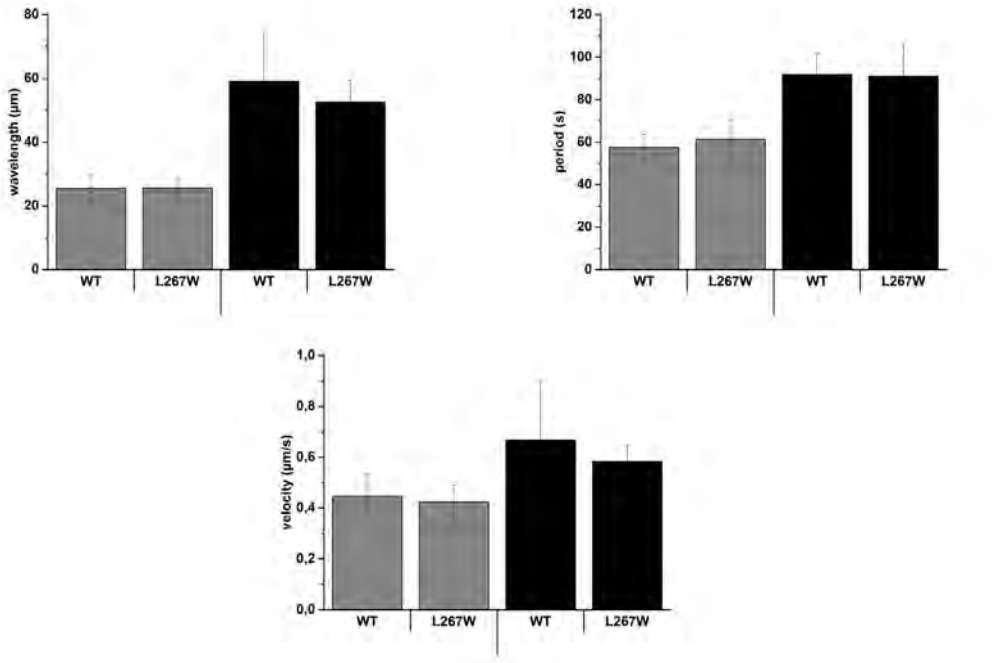

FIGURE 3.7: Wavelength, period, and velocity of regular patterns formed by MinD WT and MinD L267W. Travelling waves of MinD WT and MinD L267W at MinD concentrations of 1 (grey bars) and 2 μM (black bars) in the presence of 1 μM MinE and 2.5 mM ATP were analyzed in terms of wavelength, period, and velocity. The quantitative analysis does not show a remarkable difference between WT and L267W waves. Error bars correspond to standard deviations resulting from at least three independent experiments.

The quantitative analysis of patterns formed by MinD L267W did not show any remarkable difference to MinD WT (Fig. 3.7). From my *in vitro* analysis on pattern formation, I can conclude that self-organization of MinD L267W resembled that of MinD WT.

MinD Ins3: Titrations at low absolute protein concentrations

As described in the previous section, MinD Ins3 showed some faint patterns at MinD concentrations of 0.5 and 1 μM in the presence of 1 μM MinE. However, no pattern formation occurred when MinD was titrated to higher concentrations. This behavior looked different from that of MinD WT and MinD L267W, thus it was investigated

further. I tested the effect of low absolute MinD and MinE concentrations in the system. First, I titrated MinD from 100 nM to 1 μM in the presence of a constant concentration of MinE of 1 μM. Secondly, I titrated MinE from 100 nM to 1 μM while keeping MinD concentration constant to 250 nM.

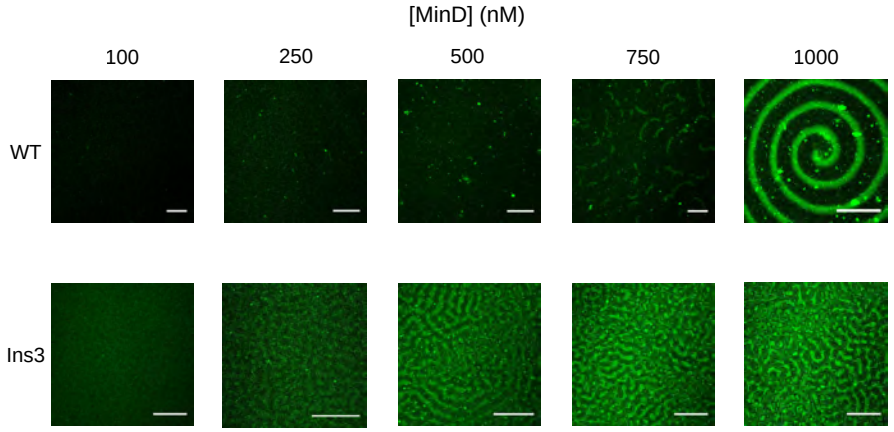

FIGURE 3.8: Self-organization of MinD WT and MinD Ins3 on SLBs at increasing MinD concentration. Total MinD concentration (70 % untagged MinD, 30 % eGFP-MinD) was titrated between 100 and 1000 nM in the presence of 1 μM MinE and 2.5 mM ATP. MinD Ins3 showed formation of standing waves at MinD concentrations of 500, 750, and 1000 nM. The formation of patterns, although faint and more disordered, was observed also at MinD concentrations of 100 and 250 nM. MinD WT formed interrupted patterns at MinD concentration of 750 nM and stable travelling waves at MinD concentration of 1000 nM. The experiment was run in triplicate. Scale bar: 50 μm.

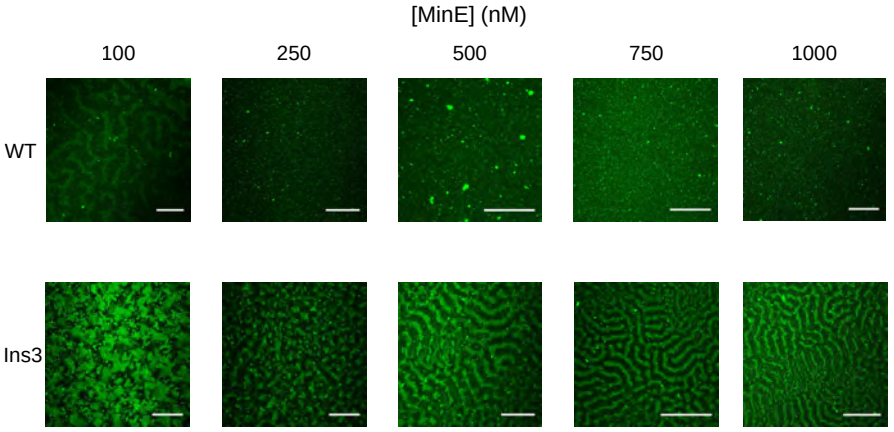

FIGURE 3.9: Self-organization of MinD WT and MinD Ins3 on SLBs at increasing MinE concentration. MinE concentration was titrated between 100 and 1000 nM in the presence of 250 nM MinD (70 % untagged MinD, 30 % eGFP-MinD) and 2.5 mM ATP. MinD Ins3 showed formation of standing waves at MinE concentrations of 500, 750, and 1000 nM. The formation of disordered patterns was observed at MinE concentrations of 100 and 250 nM. MinD WT did not show self-organization when MinE was titrated between 250 and 1000 nM. However, in some experiments the formation of interrupted patterns was observed at MinE concentration of 100 nM. The experiment was run in triplicate. Scale bar: 50 μm.

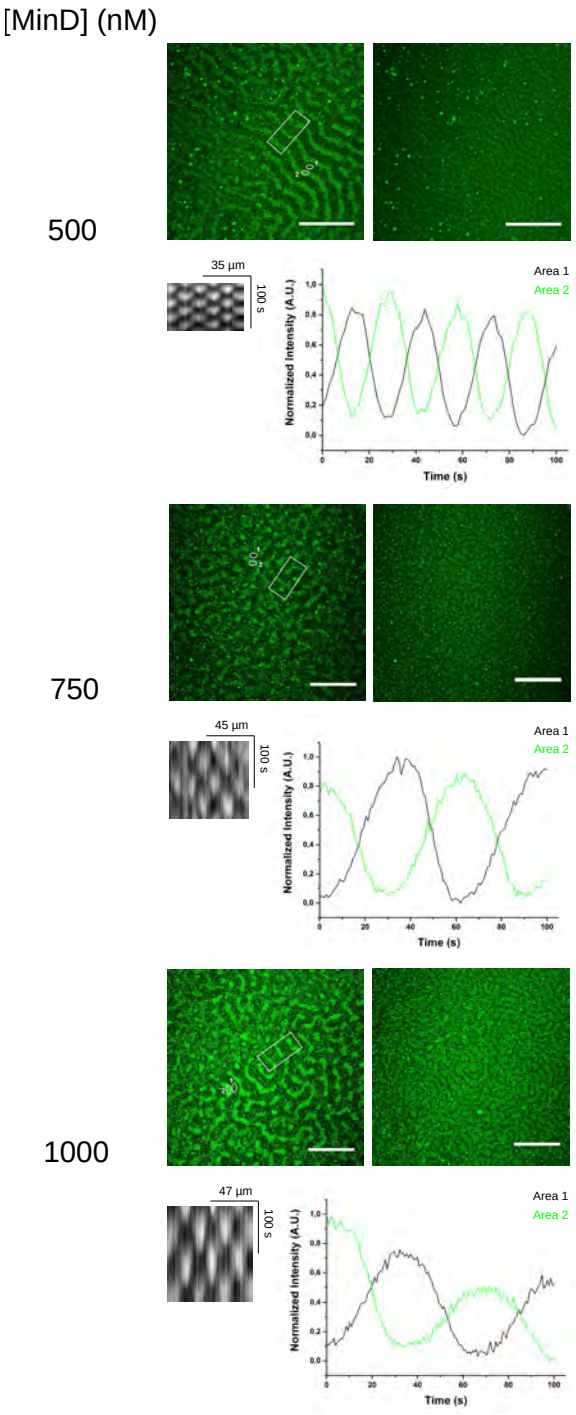

FIGURE 3.10: MinD Ins3 self-organization into oscillating standing waves at low MinD protein concentrations. MinD Ins3 self-organized into oscillating standing waves on SLBs at MinD concentrations of 500, 750, 1000 nM (70 % untagged MinD, 30 % eGFP-MinD) in the presence of 1 μM MinE and 2.5 mM ATP. For each MinD protein concentration the following is shown: a representative image of the pattern (upper left), the signal intensity averaged over a time of 100 s (upper right), a kymograph along the rectangular area shown in the representative image (bottom left), the intensity profiles of the two elliptical areas shown in the representative image (bottom right). Scale bar: 50 μm.

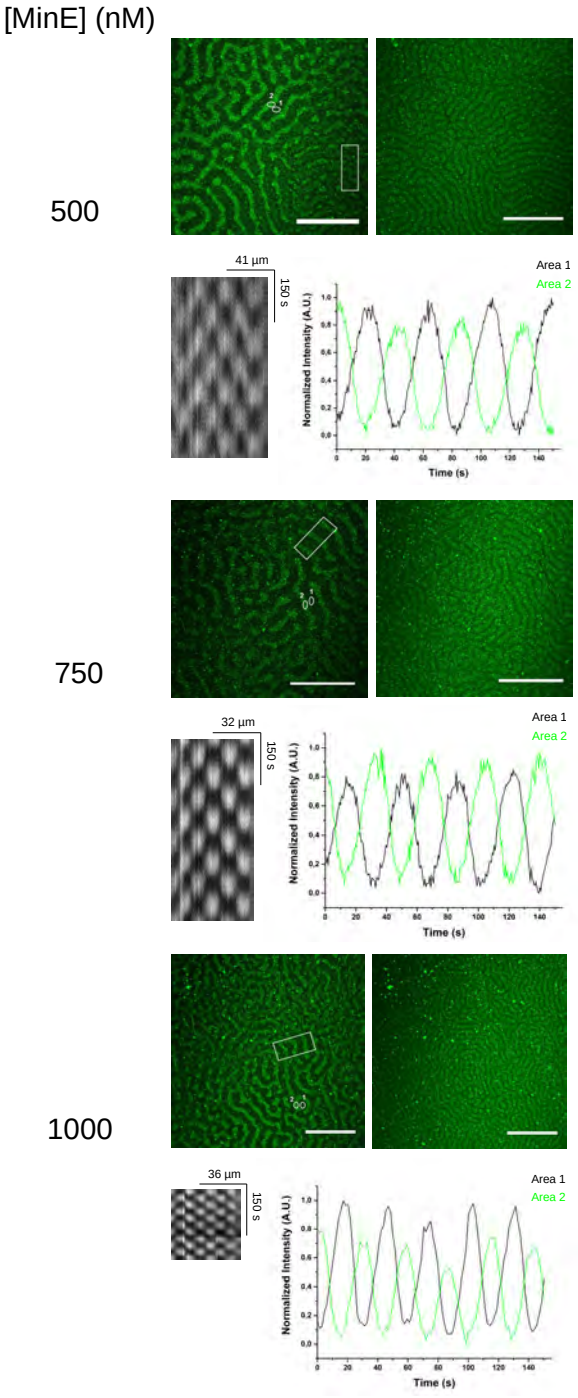

FIGURE 3.11: MinD Ins3 self-organization into oscillating standing waves at low MinE protein concentrations. MinD Ins3 self-organized into oscillating standing waves on SLBs at MinE concentrations of 500, 750, 1000 nM in the presence of 250 nM MinD (70 % untagged MinD, 30 % eGFP-MinD) and 2.5 mM ATP. For each MinE protein concentration the following is shown: a representative image of the pattern (upper left), the signal intensity averaged over a time of 150 s (upper right), a kymograph along the rectangular area shown in the representative image (bottom left), the intensity profiles of the two elliptical areas shown in the representative image (bottom right). Scale bar: 50 μm.

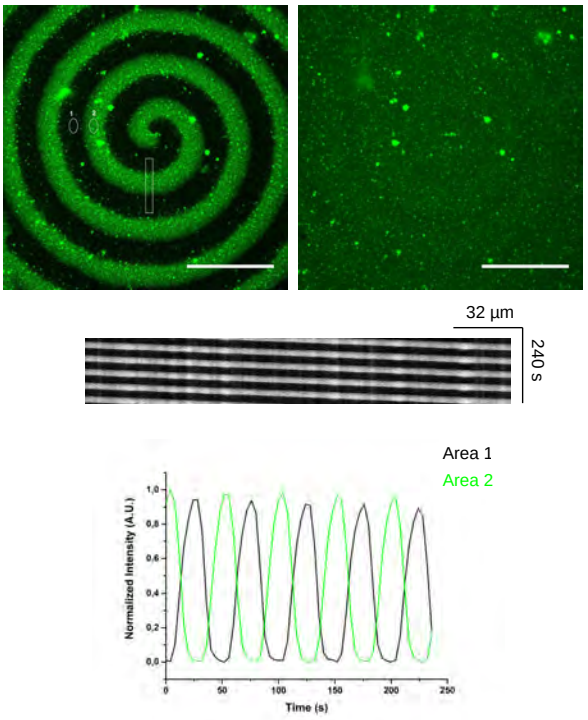

FIGURE 3.12: WT self-organization into travelling waves. MinD WT self-organized into travelling waves on SLBs at MinD concentration of 1 μM (70 % untagged MinD, 30 % eGFP-MinD) in the presence of 1 μM MinE and 2.5 mM ATP. Top: spiral pattern (left) and signal intensity of the pattern averaged over a time of 240 s (right). Middle: kymograph along the rectangular area shown in the upper left image. Bottom: intensity profiles of the two elliptical areas shown in the upper left image. Scale bar: 50 μm.

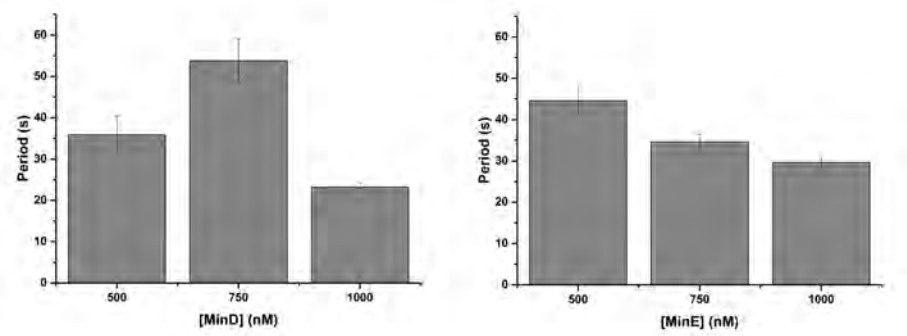

FIGURE 3.13: Oscillation period of standing waves formed by MinD Ins3 at different MinD and MinE protein concentrations. Period of the oscillating standing waves measured at MinD concentrations of 500, 750, 1000 nM (70 % untagged MinD, 30 % eGFP-MinD) in the presence of 1 μM MinE (left) and at MinE concentrations of 500, 750, 1000 nM in the presence of 250 nM MinD (70 % untagged MinD, 30 % eGFP-MinD) (right). Error bars correspond to standard deviations resulting from two independent experiments. Experiments at 1000 nM MinD and 1000 nM MinE were run only once; in these cases, error bars correspond to the standard deviation of the period measured in different parts of the sample and averaged.

The results were surprising. The first, striking observation was that the patterns were completely different from the ones formed by MinD WT, MinD L267W, or any other mutants previously tested in the group (Simon Kretschmer, unpublished data). Instead of travelling waves (formed by MinD WT), MinD Ins3 formed standing waves at specific MinD and MinE centrations. Regular, oscillatory standing waves were observed at MinD concentrations of 500, 750, and 1000 nM in the presence of 1 μM MinE and at MinE concentrations of 500, 750, and 1000 nM in the presence of 250 nM MinD (Fig. 3.8 and Fig. 3.9). Interestingly, patterns with similar shapes formed also at lower MinD and MinE concentrations of 100 and 250 nM. However, patterns at lower protein concentrations were not very regular in their spatiotemporal properties. It is important to point out that standing waves on average took longer to form than travelling waves formed by MinD WT (roughly 1 h versus 30 min). When I initially tested MinD Ins3 in comparison with MinD WT and MinD L267W I probably did not wait enough time for the patterns to form, and this can explain why I did not observe the formation of standing waves at MinD concentrations of 0.5 and 1 μM (Fig. 3.5). After the patterns were formed and regularity was reached, however, the standing waves were stable for days at RT, comparable to WT patterns.

Another remarkable difference from MinD WT was observed: MinD Ins3 seemed to show "discrete", oscillatory behavior in attaching/detaching from the membrane, rather than "continuous" like MinD WT (Fig. 3.10, 3.11, 3.12). When fluorescence intensity was averaged over time, black, unoccupied "grooves" on the membrane were a hint of discrete oscillations: zones to which the mutant never attached during its cycle of membrane binding and unbinding.

The oscillation period of regular standing waves increased with higher MinD/MinE concentration ratios (Fig. 3.13). I observed the same trend for travelling waves when titrating MinD WT and MinD L267W (Fig. 3.7), and this is known from the literature [31]. The explanation likely resides in the role of MinE in the system: the higher the MinE concentration, the higher the detachment of MinD from the membrane, thus the faster I expect the oscillation to be. The trend seemed not to be maintained at MinD and MinE concentrations of 1 μM, though (Fig. 3.13). Nevertheless, data on the oscillation period at MinD and MinE concentrations of 1 μM is the result of one single experiment. The experiment needs to be repeated before drawing definite conclusions.

MinD Ins3: Range of pattern formation

It was evident that MinD Ins3 was able to form patterns at different protein concentrations than the WT. However, the complete concentration range in which pattern formation occurred was not clear yet. I investigated the protein concentration range for

pattern formation with a further titration experiment. I started with a MinD concentration of 500 nM in the presence of 1 μM MinE and I increased the MinD concentration until I did not observe pattern formation anymore (Fig. 3.14). I performed the same experiments with MinE, starting from an initial concentration of 10 nM in the presene of 250 nM MinD (Fig. 3.15).

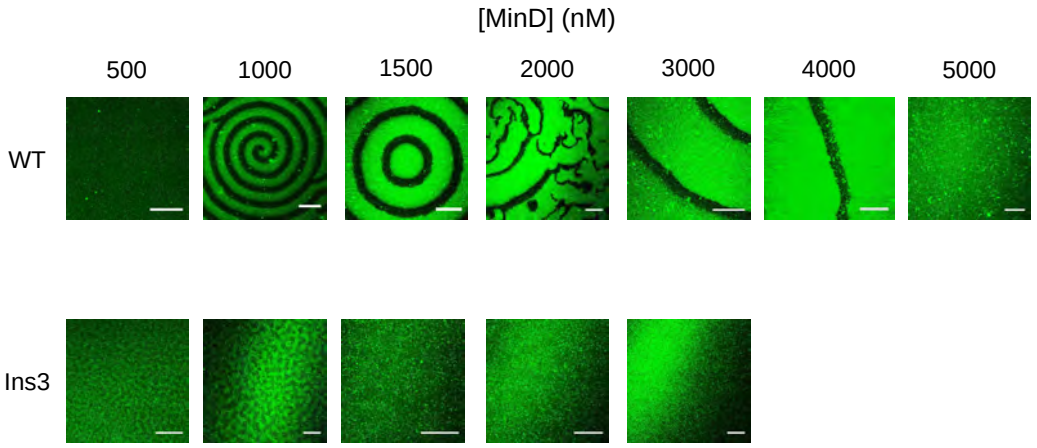

FIGURE 3.14: MinD protein concentration range for pattern formation of MinD WT and MinD Ins3. Starting from a concentration of 500 nM (70 % untagged MinD, 30 % eGFP-MinD), MinD was titrated until self-organization of MinD WT and MinD Ins3 did not occur anymore. MinD was titrated in the presence of 1 μM MinE and 2.5 mM ATP. Scale bar: 50 μm.

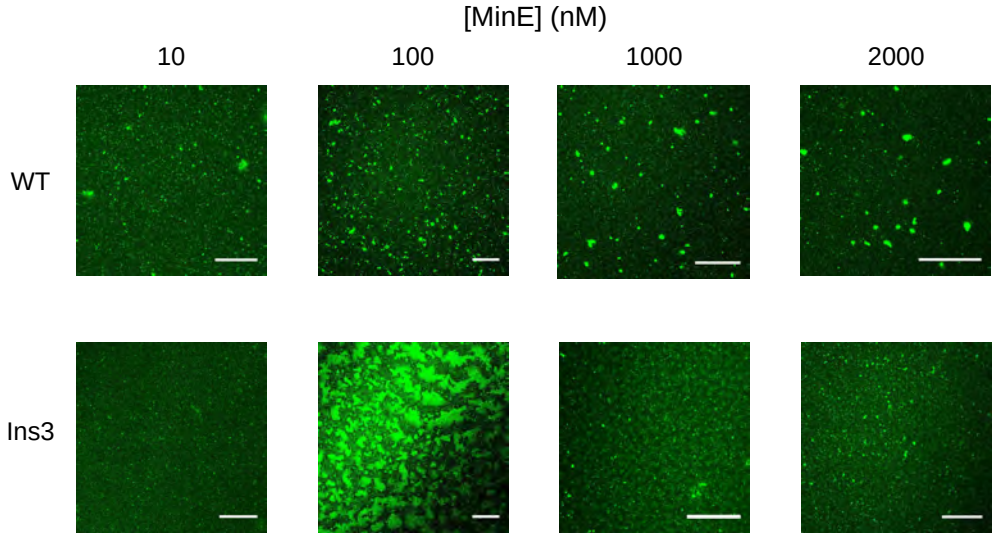

FIGURE 3.15: MinE protein concentration range for pattern formation of MinD WT and MinD Ins3. MinE protein concentration was titrated from 10 to 2000 nM in the presence of 250 nM MinD (70 % untagged MinD, 30 % eGFP-MinD) and 2.5 mM ATP. Scale bar: 50 μm.

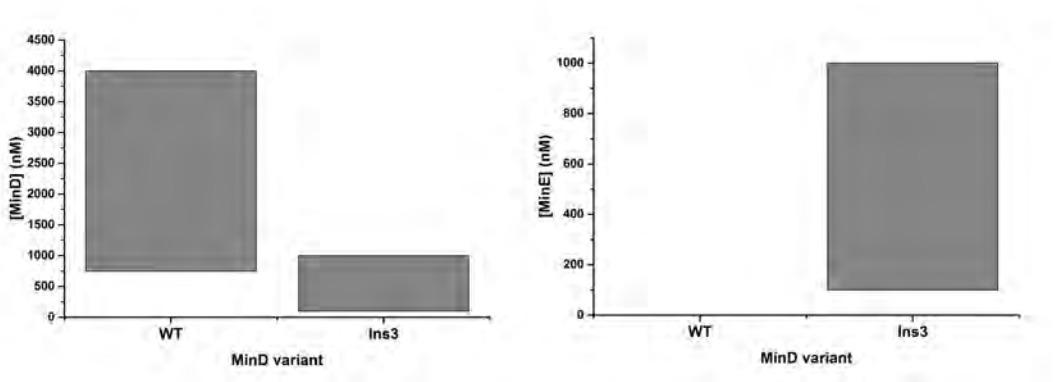

FIGURE 3.16: MinD and MinE protein concentration ranges for pattern formation of MinD WT and MinD Ins3. MinD Ins3 forms patterns in a narrower MinD concentration range with respect to MinD WT when MinD is titrated in the presence of 1 μM MinE (left). Ins3 forms patterns when MinE is titrated between 100 and 1000 nM in the presence of 250 nM MinD, while WT does not (right).

Overall, MinD Ins3's ability to form patterns was restricted to a narrower and lower concentration range with respect to MinD WT (Fig. 3.16).

3.2 ATPase mutants

MinD R3E, I4Q, 3aaNT carried mutations at the extreme N-terminus of MinD. This part of the protein is in close sequence proximity to the deviant Walker A motif, responsible for ATP binding and regulation of MinD's ATPase activity. Szeto, J., *et al.* (2004) suggested that the extreme N-terminus of MinD may also play a role in modulating the ATPase activity [47]. To confirm this suggestion, I first tested the ATPase activity of MinD R3E, I4Q, and 3aaNT. I then studied the *in vitro* self-organization of the mutants to verify whether modulation of the ATPase activity may lead to a modulation in pattern formation.

3.2.1 ATPase activity assay

MinD ATPase mutants were tested for their ability to hydrolyze ATP (Fig. 3.17). The assay was performed as described in Section 2.4.3. The ATPase activity was tested both in the presence and absence of MinE.

MinD R3E showed a higher basal ATPase activity compared to the WT; however, this high activity did not appear to be further stimulated by MinE. In fact, none of the mutants showed MinE-stimulated ATPase activity. Both in the presence and absence of MinE, ATPase activities of MinD I4Q and MinD 3aaNT were comparable to the basal

activity of MinD WT (Fig. 3.17). These results indicated that MinE was not able to stimulate MinD's enzymatic activity for the tested ATPase mutants.

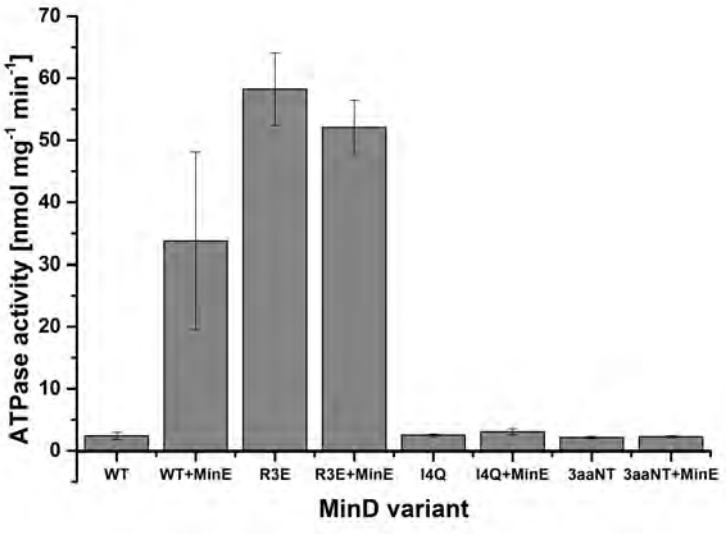

FIGURE 3.17: ATPase activity of MinD ATPase mutants. 4 μM MinD WT, R3E, I4Q, 3aaNT were incubated with and without MinE (4 µM) in the presence of phospholipid vesicles (0.2 mg/mL) in a coupled enzymatic activity assay. Error bars correspond to standard deviations resulting from three independent experiments.

3.2.2 Self-organization assays

As for the membrane binding mutants, the effect of MinD protein concentration on pattern formation was also investigated for the ATPase mutants. The following MinD concentrations were tested: 0.5, 1, 2, 3 μM MinD in the presence of 1 μM MinE.
None of the ATPase mutants showed pattern formation on SLBs at any of the tested MinD concentrations (Fig. 3.18). Interestingly, MinD 3aaNT did not appear to bind to the membrane at any tested MinD concentration; this was further demonstrated by looking at Z-scans (Fig. 3.19).

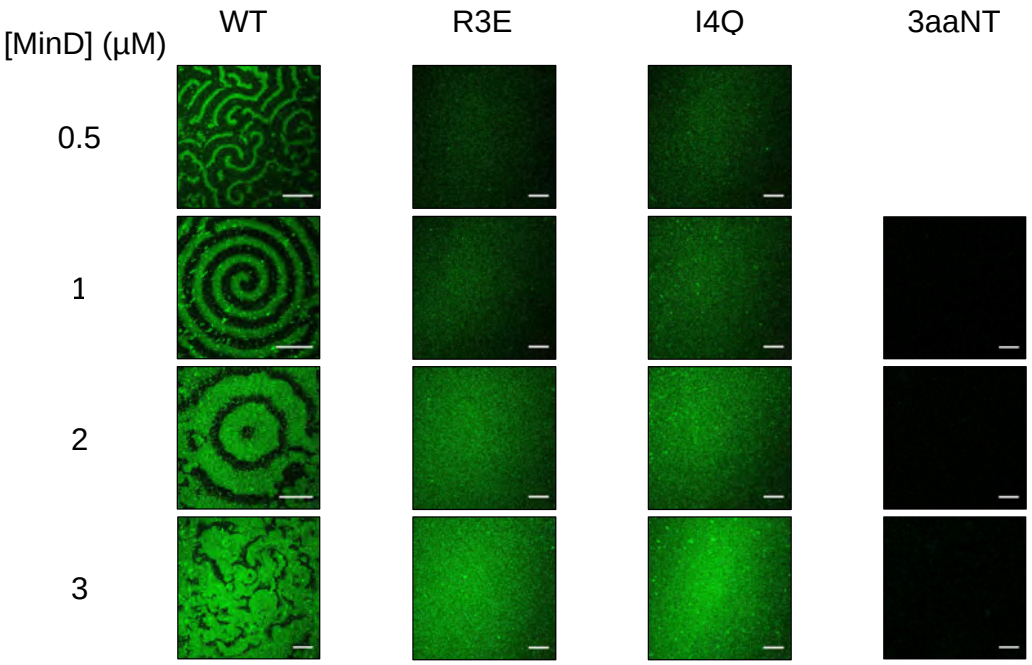

FIGURE 3.18: Lack of self-organization of MinD ATPase mutants at various MinD concentrations. eGFP-tagged MinD WT, R3E, I4Q, 3aaNT were observed on SLBs and did not show self-organization at any tested MinD concentration. Total MinD concentration (70 % untagged MinD, 30 % eGFP-MinD) was titrated between 0.5 and 3 μM in the presence of 1 μM MinE and 2.5 mM ATP. Scale bar: 50 μm. This experiment was performed only once due to time constraints.

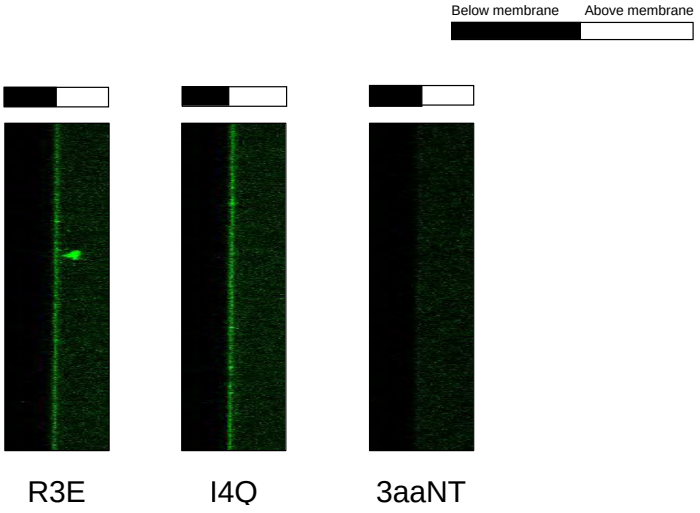

FIGURE 3.19: Z-scans of MinD ATPase mutants. Z-scans of eGFP-tagged MinD R3E, I4Q, 3aaNT (0.15 μM) incubated on SLBs in the presence of 1 μM MinE and 2.5 mM ATP. Untagged MinD was also added to a total MinD concentration of 0.5 μM. This experiment was performed only once due to time constraints.

Chapter 4

Conclusions

4.1 Discussion

4.1.1 Membrane affinity and pattern formation of MinD L267W is similar to MinD WT

Substitution of MinD L-267 with a tryptophan residue did not appear to affect MinD self-organization. Patterns formed by MinD L267W on SLBs looked very similar to those formed by MinD WT (Fig. 3.5 and 3.6). Moreover, a quantitative analysis of the patterns did not reveal a significative difference between MinD L267W and MinD WT in terms of wavelength, period, and velocity of the travelling waves (Fig. 3.7). These findings were unexpected. As mentioned previously, MinD L267W was suggested to bind membranes less efficiently than MinD WT; moreover, MinD L267W's stimulated ATPase activity was reported to be lower than that of MinD WT [43].

Interestingly, my results about MinD L267W's ATPase activity were discordant with the data reported by Zhou, H., *et al.* (2003): rather than lower, MinD L267W's MinE-stimulated ATPase activity was higher than MinD WT's activity from my experiments in the presence of MinE and lipid vesicles (Fig. 3.4) [43]. However, two different types of assay were performed: Zhou, H., *et al.* (2003) measured the release of γ-^{32}P from γ-^{32}P-labeled ATP at two different time points rather than following the decrease of NADH absorbance over time with a coupled enzymatic assay. Moreover, the group tested higher concentrations of MinD and MinE than I did [43]. It would be interesting to test MinD L267W's ATPase activity via the coupled enzymatic assay with higher protein concentrations to assess whether, in these conditions, MinD L267W's enzymatic activity is consistent with the results from the literature.

Furthermore, MinD L267W was suggested to have weaker binding affinity for membranes

than MinD WT [43]. From the results of my microscopy and biochemical experiments, affinity of MinD L267W for membranes does not appear different from MinD WT (Fig. 3.2 and 3.3). However, membrane-binding was assessed only via qualitative assays. A follow-up experiment could be measuring membrane binding in a quantitative way, for example comparing fluorescent signals using Z-scans and well-defined laser settings or applying sophisticated kinetic techniques.

An interesting observation is that tryptophan residues are more bulky than leucine residues. Due to this factor, it is possible that *in vivo* MinD L267W binds membranes preferentially at the cell poles. Preferential binding in the presence of membrane curvature may eventually affect Min oscillations that, on the other hand, may not be altered in a setup lacking spatial cues, such as SLBs. Although beyond the purposes of my project, it would be interesting to test this hypothesis *in vivo*. As an alternative, in *in vitro* studies the mutant may be tested in PDMS compartments resembling *E. coli* cell shape.

Interestingly, patterns formed by MinD WT and MinD L267W show a concentration dependence: travelling waves are affected in terms of wavelength, period, and velocity when MinD concentration is increased from 1 μM to 2 μM in the presence of 1 μM MinE (Fig. 3.7). The qualitative appearance of the waves changes as well (Fig. 3.6). The higher the MinD/MinE ratio, the thicker the waves. Furthermore, target patterns are more frequently observed than spiral patterns at higher MinD/MinE ratio. These findings are consistent with other mutants previously tested in the group (Simon Kretschmer, unpublished data). Although noticeable from experimental results, the latter phenomenon would need deeper theoretical studies for a rational explanation of the dynamics.

4.1.2 MinD L267E is unable to bind lipid membranes and support pattern formation

In accordance with findings by Zhou, H., *et al.* (2003) and Szeto, T., *et al.* (2002), MinD L267E did not display membrane-binding ability (Fig. 3.2 and 3.3) [40, 43]. As pattern formation did not occur for this mutant over a range of MinD concentrations, this highlights the fundamental role of MinD membrane binding for the Min system's dynamic behavior. Furthermore, the mutant's behavior is a good corroboration of the results from the literature, and it could be used as a useful negative control for future experiments on MinD membrane binding.

4.1.3 Abrogation of stimulation of MinD's ATPase activity leads to loss of self-organization

MinD R3E, I4Q, and 3aaNT carry mutations in the N-terminus of MinD. These mutants did not display MinE-stimulated ATPase activity (Fig. 3.17). MinE's inability to stimulate the ATPase activity of the mutants very likely accounts for the absence of self-organization on SLBs (Fig. 3.18). In fact, even in the case of MinD R3E (which presents high basal ATPase activity but absence of stimulation by MinE), pattern formation does not occur. These results confirm that MinE's stimulation of MinD's ATPase activity is necessary for self-organization to occur. As proposed by Hu, Z., and Lutkenhaus, J. (2001), the stimulation of MinD's ATPase activity by MinE is a key step in driving MinD oscillation [24]. Notably, Szeto, J., *et al.* (2004) tested MinD K3E, I4Q, and 3aaNT from *Neisseria gonorrhoeae*. The three mutants were reported to display dynamic movement and oscillations *in vivo* in the presence of MinE [47].
Since the ATPase mutants did not support pattern formation, they were not investigated further. Nevertheless, it is worth giving some thoughts about the role of the extreme N-terminal region of MinD, which has been poorly characterized so far. It would be interesting to look at fluorescently tagged MinE proteins on SLBs in the presence of eGFP-tagged MinD and ATP-γ-S. This experiment would test whether the interaction between the two proteins is abolished. In case the interaction is conserved, a possible role of the residues in the N-terminus might be to transmit the effects of MinE-binding to the ATPase region. MinD residues 92-94 were previously proposed to have this role in a study of *N. gonorrhoeae* MinD [50].

4.1.4 MinD Ins3 self-organizes into standing waves on SLBs in the presence of MinE

MinD Ins3 contains a three-amino acid insertion in the MTS thus mimicking the *B. subtilis* MTS. It has been shown that one single *B. subtilis* MTS is sufficient, while two *E. coli* MTS in local proximity are necessary to promote membrane binding of GFP *in vivo* [22]. From these results, it can be assumed that MinD Ins3 binds membranes with stronger affinity than MinD WT. However, from a qualitative analysis of membrane binding, I was not able to detect a significant difference between MinD Ins3's and WT's affinities for membranes (Fig. 3.2 and 3.3). However, MinD Ins3's self-organization on SLBs was dramatically different from MinD WT. MinD Ins3 displayed a kind of oscillatory behavior not previously reported in *in vitro* studies on Min proteins: the mutant self-organizes into standing waves at certain MinD and MinE protein concentrations,

while MinD WT self-organizes into travelling waves (Fig. 3.10, 3.11, 3.12). Moreover, Ins3 displays self-organization at different MinD and MinE protein concentrations from MinD WT (Fig. 3.14).

When MinD and MinE concentrations are in the micromolar range and the MinD/MinE concentration ratio is 1:2, MinD Ins3 is not able to self-organize (Fig. E.2). However, when protein concentrations are in the range between 100 and 1000 nM MinD Ins3 self-organizes into standing waves at the same MinD/MinE concentration ratio of 1:2 (Fig. 3.8 and 3.9). These results suggest that not only relative concentrations, but also absolute protein concentrations have an influence on the dynamics.

When MinD or MinE concentration is gradually increased during titration experiments, the patterns are indistinguishable from patterns resulting from a same, initial MinD or MinE protein concentration. In other words, during titration experiments forming patterns do not seem to have a "memory" of patterns formed at lower concentrations. From this evidence it can be suggested that the system does not show concentration-dependent hysteresis.

An interesting feature of the patterns formed by MinD Ins3 is the apparent "discrete" behavior of the mutant. During its cycles of membrane binding and unbinding, MinD Ins3 seems to occupy only certain spots on the membrane, while other zones remain MinD-free (Fig. 3.10 and 3.11). It would be interesting to test where MinE localizes on the membrane. In the presence of MinD WT, MinE is known to accumulate in a structure called the E-ring [31, 34]. With the concurrent use of fluorescently tagged MinD and MinE it could be assessed whether MinE binds the membrane in the zones where MinD Ins3 seems not to bind and what shape the MinE distribution displays.

From preliminary data, the oscillation period of standing waves formed by MinD Ins3 tends to decrease with increasing MinE/MinD concentration ratio (Fig. 3.13). This is in accordance with my data on MinD WT and MinD L267W (Fig. 3.7) as well as previous studies [31], and can be explained with the role of MinE in the system: MinE stimulates MinD detachment from the membrane, therefore oscillations are expected to be faster (i.e. smaller oscillation period) at higher concentrations of MinE. However, measurements need to be repeated for a more solid assessment of the trend. Moreover, further quantitative analyses should be performed for a better comprehension of the dynamics. For example, determining MinD's rates of attachment to and detachment from the membrane (k_{on} and k_{off}) would be of great help for theoretical models of the system. Furthermore, the formation of standing waves rather than travelling waves raises questions about single-molecule behavior. Tracking single-molecules, for example in total internal reflection fluorescence (TIRF) experiments could help investigate the mechanism of membrane binding/unbinding at the molecular level. For instance, studying the diffusion of MinD on the membrane may help investigate what happens in the transition between occupied and unoccupied zones.

4.2 Outlook

From my study on MinD mutants with engineered membrane affinity or ATPase activity, MinD Ins3 displayed the most interesting features and revealed to be a promising candidate to perform further investigations on Min protein dynamics. As mentioned previously, single-molecule experiments on MinD Ins3 and MinD WT would allow to look at differences, at the molecular level, in membrane binding/unbinding. Another interesting experiment would be to investigate the self-organization of a mixed population of MinD WT and MinD Ins3. Furthermore, titration experiments aiming at identifying MinD and MinE concentration ranges necessary for pattern formation need to be repeated for more solid results. Different concentrations may also be tested upon suggestions by mathematical modelers, to test whether the ranges for self-organization can be narrowed down.
As mentioned in the introduction, MinD's membrane binding and ATPase activity are deeply interconnected functions. Therefore further investigation of MinD Ins3's ATPase activity could be relevant. The rate of ATP hydrolysis may be estimated taking into account the amount of molecules bound to the membrane, upon performing experiments to quantify MinD Ins3's membrane binding. This may help to identify whether the high stimulated ATPase activity of the mutant is due to a higher number of molecules on the membrane or to faster cycles of membrane binding and unbinding of individual proteins. Furthermore, the ATPase assay should be repeated titrating MinD and MinE concentrations: the resulting curves may carry relevant information about enzyme kinetics (e.g. the Hill coefficient may be extrapolated, which provides a way to quantify cooperativity).

The three mutants carrying mutations in the N-terminus did not show self-organization on SLBs. However, the self-organization experiment was performed only once at high absolute concentrations of MinD and MinE. As suggested by experiments on MinD Ins3, absolute protein concentrations have a role in influencing the dynamics. Therefore it would be interesting to repeat the experiment, and also test whether self-organization of these mutants occurs at low absolute protein concentrations.

Lastly, new sets of mutants may be designed and tested with the same purpose of affecting and studying Min protein pattern formation. For instance, a mutant with an altered number of positively charged residues in the MTS may be tested for weaker membrane binding. With the support of structural studies, MinD mutants may be rationally engineered to achieve a custom modulation of self-organization.

Acknowledgements

My very first and special thanks genuinely go to Petra and Simon. To Petra, who gave me the opportunity to join her lab twice: for my summer project in the first place, and then she offered me the chance to come back for my Master's thesis and continue working in the exciting field of bottom-up synthetic biology. And to Simon, who has scrupulously supervised me since the beginning of my adventure in Munich, at the same time leaving me the necessary freedom to independently organize my time and experiments. Also, I want to thank him because he was great at transmitting his knowledge and experience, from which gaining I feel now confident and ready to start my imminent future as a PhD student.
I would like to thank Katja, who also supervised me during my first two months in the lab, and who taught me how to get different insights into the Min system from her point of view of a physicist.
Thank to Michaela who, besides giving me precious advice on cloning procedures, very kindly took over the cloning of eGFP-MinD R3E and successfully completed it.
Thank to Jonas and Diego, who helped me with data analysis and experiment settings with their expertise in optics and microscopy.
In general, thank to all the lab people: Sonal, Alena, Philipp B., Diego, Jonas, Cate, Beatrice, Kristina, Sven, Daniela, Simon, Franco, Henri, Franziska, Thomas, Eugene, Martin, Matias, Ilaria (and Conrad), Gosia, Philipp G., Leon, Lei, Haiyang, Toby, Kerstin, Bea, Michaela, Brigitte, Sigrid, Frank, Helge, and Silke because every single one has always been kind, helpful, and willing to answer to any of my questions. Thank because, despite being so many, all these people together have managed to create an uncommonly comfortable and peaceful working environment, which I was extremely pleased to be part of.

For the technical support, thank to the Core facility of the institute, which expressed and purified MinD WT and eGFP-MinD WT.
I would also like to thank Jacob and Jonas from the Physics faculty of LMU, because of the interesting discussions about the theoretical modelling of the Min system.

Thank to my supervisor in Trento Sheref Mansy, who first introduced me to the exciting world of synthetic biology at the time of my Bachelor's project, and still supports me during my experience abroad.
I also want to thank Olivier Jousson and Alessandro Quattrone as representatives of the Centre for Integrative Biology (CIBIO) at the University of Trento, because of the intense, formative, last five years I have spent at the University, and because of the full support and assistance I have always received in all my projects and activities.

A warm thank goes to Cate who, despite all her (imaginary) problems, always radiates positive vibes and shares the love for "nonsense" with me, for which we've become very good friends and we've spent long times laughing both inside and outside the lab.
A huge thank goes in general to all my friends at LMU because of their easy-going mood and natural good cheer. In particular, a special thank goes to Anna and Giaco, because it was an incredible chance for the three of us to meet again somewhere in Europe, and we've made the most out of our time together.
Again thank to all the friends I've met here, because they have made these last months in Munich a special time, and to my friends in Trento, who always support me and are willing to host me every time I swing by.

Finally, an exclusive thank goes to Harry, because we've hanged in for more than one year living far apart, and now it's time to start our new adventure together in a different part of the world.

Appendix A

List of primers

TABLE A.1: List of primers. Mutations are highlighted in red. Insertions are highlighted in green. The two nucleotides surrounding nucleotide deletions are highlighted in blue and magenta.

Name	Sequence
L267E_Fwd	GGCTTCCTCAAACGCGAATTCGGAGGATAAGTT
L267E_Rev	AACTTATCCTCCGAATTCGCGTTTGAGGAAGCC
L267E_EGFP_Fwd	GGCTTCCTCAAACGCGAATTCGGAGGATAAAAG
L267E_EGFP_Rev	CTTTTATCCTCCGAATTCGCGTTTGAGGAAGCC
L267W_Fwd	GCTTCCTCAAACGCTGGTTCGGAGGATAAGT
L267W_Rev	ACTTATCCTCCGAACCAGCGTTTGAGGAAGC
L267W_EGFP_Fwd	GCTTCCTCAAACGCTGGTTCGGAGGATAAAA
L267W_EGFP_Rev	TTTTATCCTCCGAACCAGCGTTTGAGGAAGC
Ins3_Fwd	AGAAGAAAGGCTTCCTCGCGAAAATTAAACGCTTGTTCGGAGG
Ins3_Rev	CCTCCGAACAAGCGTTTAATTTTCGCGAGGAAGCCTTTCTTCT
I4Q_Fwd	TCCGAATTCGCACGCCAGATTGTTGTTACTTCG
I4Q_Rev	CGAAGTAACAACAATCTGGCGTGCGAATTCGGA
I4Q_EGFP_Fwd	AAGGAATTCGCACGCCAGATTGTTGTTACTTCG
I4Q_EGFP_Rev	CGAAGTAACAACAATCTGGCGTGCGAATTCCTT
3aaNT_Fwd	TGGGTCGCGGATCCGAATTCATTATTGTTGTTACTTCGGG
3aaNT_Rev	CCCGAAGTAACAACAATAATGAATTCGGATCCGCGACCCA
3aaNT_EGFP_Fwd	ACGAGCTGTACAAGGAATTCATTATTGTTGTTACTTCGGG
3aaNT_EGFP_Rev	CCCGAAGTAACAACAATAATGAATTCCTTGTACAGCTCGT

Appendix B

Mutagenesis protocols

B.1 *In vitro* one site-directed mutagenesis

Table B.1: Reaction mix for *In vitro* one site-directed mutagenesis

Component	**Volume (μL)**	**Final concentration**
10X AccuPrime^{TM} *Pfx* Reaction Mix	5	1X
10X PCR enhancer	5	1X
10 μM Primer 1	1.5	0.3 μM
10 μM Primer 2	1.5	0.3 μM
50 ng/μL Plasmid DNA	1	-
4 U/μL DNA Methylase	2	1X
25X SAM (S-adenosyl methionine)	2	1X
2.5 U/μL AccuPrime^{TM} *Pfx* DNA Polymerase	0.4	1 U
PCR water	to 50	-

Table B.2: Methylation reaction and site-directed mutagenesis PCR

Temperature (°C)	**Duration**	**Number of cycles**
37	20 min	1
94	2	
94	20 s	18
57	30 s	
68	3.5 min	
68	5	1
4	forever	1

Table B.3: Components for recombination reaction

Component	**Volume (μL)**	**Final concentration**
5X Reaction Buffer	4	1X
PCR water	10	-
PCR sample	4	-
10X Enzyme Mix	2	1

The recombination reaction was performed for 10 min at room temperature (RT). The reaction was stopped by adding 1 μL 0.5 M Ethylenediaminetetraacetic acid (EDTA) before proceeding with transformation. 2 μL of each recombination reaction were transferred into one 50-μL vial of OneShot® MAX Efficiency® DH5α^{TM}-T1® competent cells. The vials were incubated on ice for 20 min. Thermal shock was performed by incubating the vials in a water bath for 30 s at 42 °C and then the vials were covered with ice for 2 min. 250 μL sterile Super Optimal Broth (SOC) medium were added to each vial and the vials were incubated for 1 h at 37 °C at 500 rpm. The cell suspension was diluted 1:10 and 100 μL of diluted cells were plated on LB Kan agar plates. Plates were incubated O/N at 37 °C. Then, 3 to 5 colonies were selected for each plate and plasmid DNA was purified using either QIAprep Spin Miniprep Kit (QIAGEN) or perGOLD Plasmid Miniprep Kit I (Peqlab). Plasmid DNA sequence was analyzed by sequencing (Max-Planck-Institut für Biochemie - Martinsried - DNA sequencing facility).

B.2 Temperature gradient site-directed mutagenesis

The protocol consists of two gradient PCRs. 3 different temperatures were tested for each construct. One tube with the reaction mix was prepared for each temperature. In the first PCR, each tube contained only one primer (either forward or reverse). After the first PCR, 25 μL of the content of tubes of the respective temperature were mixed together. 1 μL Phusion DNA polymerase (2 U/μL, Thermo Scientific) was added and a second PCR was run.

Table B.4: Reaction mix for temperature gradient site-directed mutagenesis

Component	**Volume (μL)**	**Final concentration**
5X Phusion GC buffer	10	1X
25 mM dNTPs	2	1 mM
50 mM $MgCl_2$	2	2 mM
100 ng/μL Plasmid DNA	1	-
100 % DMSO	0.8	-
100 pmol/μL Primer	0.2	4 pmol/μL
2 U/μL Phusion DNA Polymerase	1	1 U
PCR water	to 50	-

Table B.5: First PCR conditions for temperature gradient site-directed mutagenesis

Temperature (°C)	**Duration**	**Number of cycles**
98	5 min	1
98	45 s	
50-65	45 s	10
72	3.5 min	
4	forever	1

Table B.6: Second PCR conditions for temperature gradient site-directed mutagenesis

Temperature (°C)	**Duration**	**Number of cycles**
98	3 min	1
98	45 s	
50-65	45 s	18
72	4 min	
4	forever	1

Each PCR product was then digested by adding 1.5 μL DpnI (10 U/μL, Thermo Scientific). The tubes were incubated for 1 h at 37 °C. The restriction digest reaction was stopped by incubating the tubes for 15 min at 80 °C. 3 μL of each restriction digest reaction were then transferred into one 50-μL vial of OneShot® MAX Efficiency® DH5α^{TM}-T1® competent cells. The vials were incubated on ice for 20 min. Thermal shock was performed by incubating the vials in a water bath for 1 min at 42 °C and then the vials were covered with ice for 2 min. 200 μL sterile SOC medium were added to each vial and the vials were incubated for 1 h at 37 °C at 500 rpm. The whole cell suspension was plated on LB Kan agar plates. Plates were incubated O/N at 37 °C. Then, 3 to 5 colonies were selected for each plate and plasmid DNA was purified using either QIAprep Spin Miniprep Kit (QIAGEN) or perGOLD Plasmid Miniprep Kit I (Peqlab).

Finally, plasmid DNA sequence was analyzed by sequencing (Max-Planck-Institut für Biochemie - Martinsried - DNA sequencing facility).

Appendix C

Protein concentrations

Protein concentrations were assessed via Bradford assay. The Dye Reagent Concentrate (Bio-Rad) was diluted 1:4 with millipore water and filtered with a disposable vacuum-driven filtration system (Steriflip®). Five dilutions of bovine serum albumin (BSA) protein standard were prepared (100, 250, 500, 1000, and 2000 μg/mL) and 2.5 μL of each standard and sample solution were pipetted into separate microtiter plate wells. Sample and standard solutions were assayed in duplicate. 200 μL of the diluted Dye Reagent were added to each well and the plate was incubated for 30 min at RT while shaking. Then, absorbance was measured at 595 nm with a TECAN infinite M200 PRO microplate reader. Protein concentrations were extrapolated from the resulting standard curve.

Table C.1: Protein concentrations estimated via Bradford assay.

Protein	**Concentration (μM)**
MinD L267E	43.6
eGFP-MinD L267E	41.9
MinD L267W	32.4
eGFP-MinD L267W	39.9
MinD Ins3	20.2
eGFP-MinD Ins3	16.2
MinD R3E	24.6
eGFP-MinD R3E	25.3
MinD I4Q	18.2
eGFP-MinD I4Q	22.2
MinD 3aaNT	32
eGFP-MinD 3aaNT	23.3
MinD WT	33.5
eGFP-MinD WT	18.3
MinE	131.1

Appendix D

Chromatographic fractions

Mutations in the MinD MTS were expected to affect MinD binding to lipid membranes. To assess whether the solubility of the proteins was affected, SDS-PAGE with the purification fractions of eGFP-tagged MinD membrane-binding mutants were run.

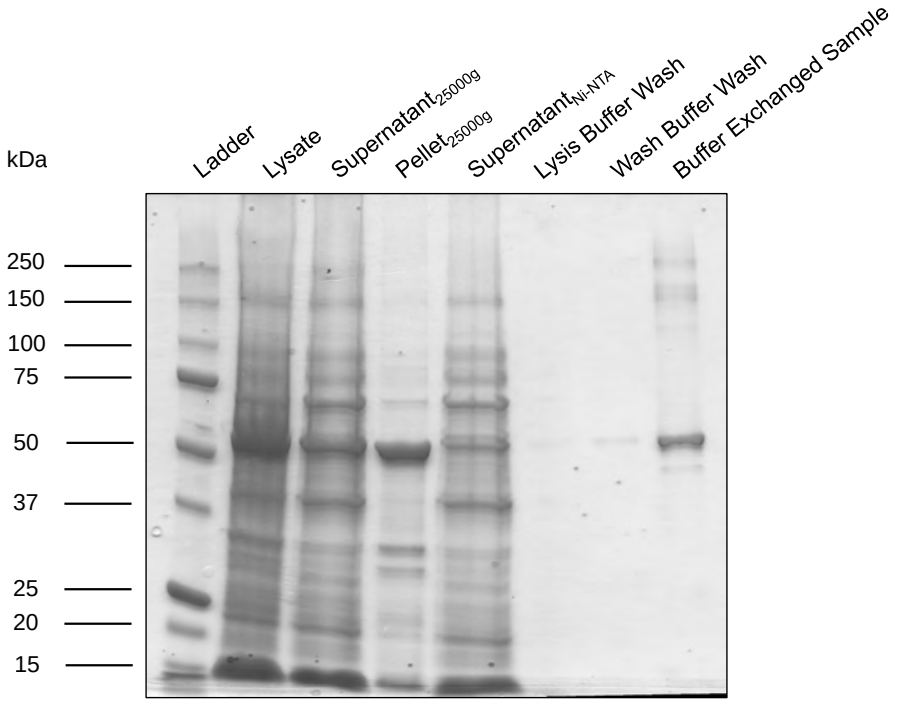

FIGURE D.1: Coomassie stained polyacrilamide gel with purification fractions of eGFP-MinD L267E. Samples of fractions were collected during the purification process and loaded on a polyacrilamide gel. Samples were diluted 1:10 for a better visualization of protein bands. Loading volumes of samples were adjusted according to their degree of dilution. Mass of eGFP-MinD L267E is 60.1 kDa.

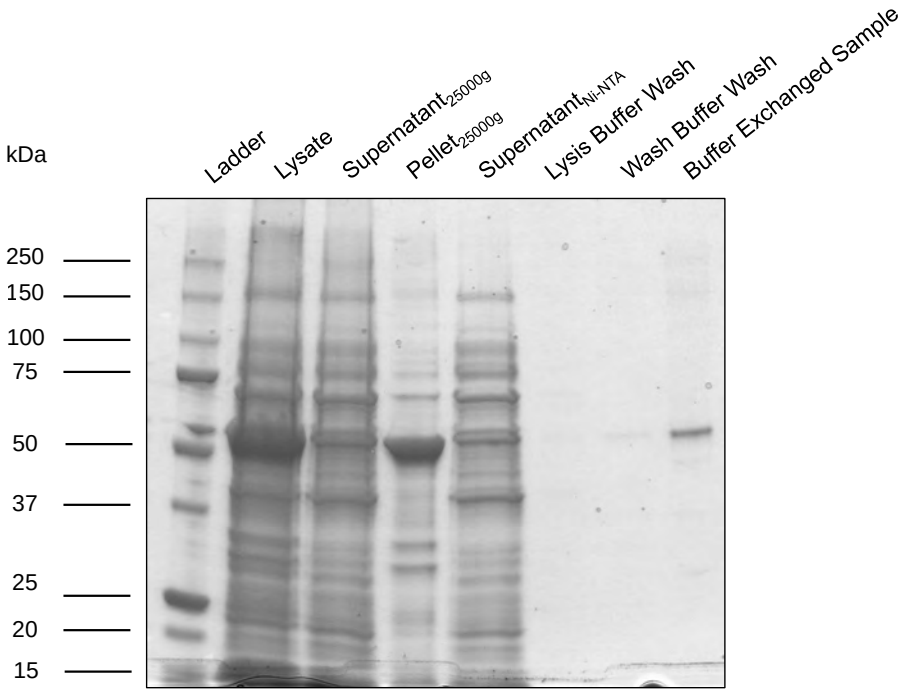

FIGURE D.2: Coomassie stained polyacrilamide gel with purification fractions of eGFP-MinD L267W. Samples of fractions were collected during the purification process and loaded on a polyacrilamide gel. Samples were diluted 1:10 for a better visualization of protein bands. Loading volumes of samples were adjusted according to their degree of dilution. Mass of eGFP-MinD L267W is 60.2 kDa.

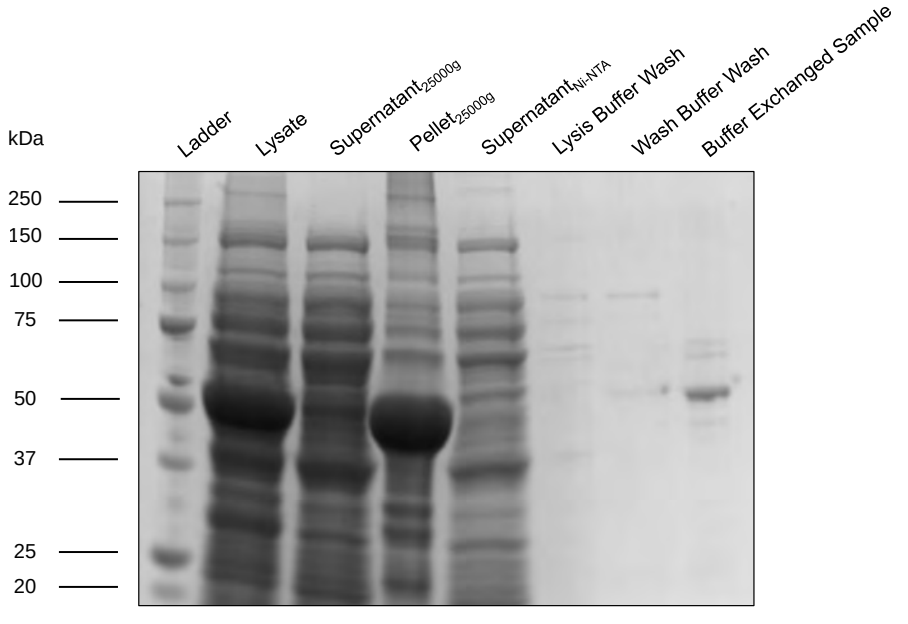

FIGURE D.3: Coomassie stained polyacrilamide gel with purification fractions of eGFP-MinD Ins3. Samples of fractions were collected during the purification process and loaded on a polyacrilamide gel. Loading volumes of samples were adjusted according to their degree of dilution. Mass of eGFP-MinD Ins3 is 60.4 kDa.

Appendix E

Results - Lack of self-organization

E.1 Z-scans of MinD L267E at various MinD concentrations

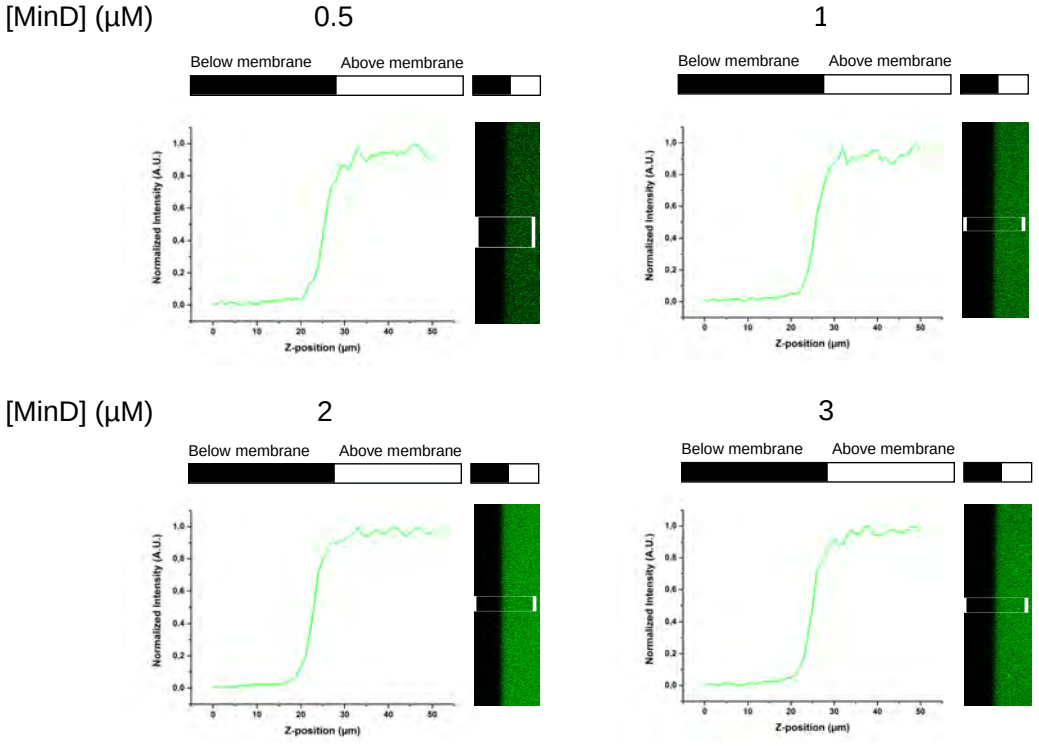

FIGURE E.1: Z-scans of MinD L267E at various MinD concentrations in the presence of MinE. MinD was titrated at the following concentrations: 0.5, 1, 2, 3 μM (70 % untagged MinD, 30 % eGFP-MinD) in the presence of 1 μM MinE and 2.5 mM ATP. For each MinD concentration the following is shown: Z-scan of eGFP-MinD L267E incubated on SLBs (right) and corresponding profiles (left) along the rectangular area shown in the Z-scan.

E.2 Self-organization assay of MinD Ins3 at "high" absolute MinE concentrations

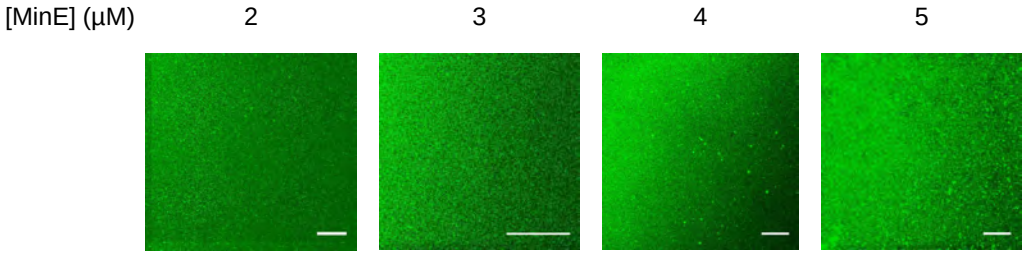

FIGURE E.2: Self-organization assay of MinD Ins3 on SLBs in the presence of various MinE concentrations in the micromolar range. MinE was titrated from 2 to 5 μM in the presence of 1 μM MinD Ins3 (70 % untagged MinD, 30 % eGFP-MinD) and 2.5 mM ATP. Scale bar: 50 μm.

Bibliography

[1] Petra Schwille. Bottom-up synthetic biology: engineering in a tinkerer's world. *Science*, 333(6047):1252–1254, 2011.

[2] Scott Camazine. *Self-organization in biological systems*. Princeton University Press, 2003.

[3] Eric Karsenti. Self-organization in cell biology: a brief history. *Nature Reviews Molecular Cell Biology*, 9(3):255–262, 2008.

[4] James Dickson Murray. Mathematical biology. i: An introduction. ii: Spatial models and biomedical applications. *Interdisciplinary Applied Mathematics*, 17, 2002.

[5] Alfred Gierer and Hans Meinhardt. A theory of biological pattern formation. *Kybernetik*, 12(1):30–39, 1972.

[6] Philip K Maini, Ruth E Baker, and Cheng-Ming Chuong. The Turing model comes of molecular age. *Science (New York, NY)*, 314(5804):1397, 2006.

[7] Animalia Life. http://animalia-life.com/leopard.html, Accessed: 2015-09-21.

[8] Pattern formation and dynamics in nonequilibrium systems. http://physics.wooster.edu/Manz/gallery-nature.html, Accessed: 2015-09-21.

[9] Teach Wild. http://teachwild.org.au/school-b-2, Accessed: 2015-09-21.

[10] Australian Traveller. http://www.australiantraveller.com/4wd/032-conquer-the-sand-dunes-of-the-simpson/, Accessed: 2015-09-21.

[11] HI Adler, WD Fisher, A Cohen, and Alice A Hardigree. Miniature *Escherichia coli* cells deficient in DNA. *Proceedings of the National Academy of Sciences of the United States of America*, 57(2):321, 1967.

[12] Joe Lutkenhaus, Sebastien Pichoff, and Shishen Du. Bacterial cytokinesis: from Z-ring to divisome. *Cytoskeleton*, 69(10):778–790, 2012.

[13] Eva Nogales, Kenneth H Downing, Linda A Amos, and Jan Löwe. Tubulin and FtsZ form a distinct family of GTPases. *Nature Structural & Molecular Biology*, 5 (6):451–458, 1998.

[14] E Bi, K Dai, S Subbarao, B Beall, and J Lutkenhaus. FtsZ and cell division. *Research in microbiology*, 142(2):249–252, 1991.

[15] Sebastien Pichoff and Joe Lutkenhaus. Unique and overlapping roles for ZipA and FtsA in septal ring assembly in *Escherichia coli*. *The EMBO journal*, 21(4):685–693, 2002.

[16] Mirjam EG Aarsman, André Piette, Claudine Fraipont, Thessa MF Vinkenvleugel, Martine Nguyen-Distèche, and Tanneke den Blaauwen. Maturation of the *Escherichia coli* divisome occurs in two steps. *Molecular microbiology*, 55(6):1631–1645, 2005.

[17] Ling Juan Wu and Jeff Errington. Nucleoid occlusion and bacterial cell division. *Nature Reviews Microbiology*, 10(1):8–12, 2012.

[18] Zonglin Hu and Joe Lutkenhaus. Topological regulation of cell division in *Escherichia coli* involves rapid pole to pole oscillation of the division inhibitor MinC under the control of MinD and MinE. *Molecular microbiology*, 34(1):82–90, 1999.

[19] Zonglin Hu and Joe Lutkenhaus. Analysis of MinC reveals two independent domains involved in interaction with MinD and FtsZ. *Journal of bacteriology*, 182(14):3965–3971, 2000.

[20] Joe Lutkenhaus. Assembly dynamics of the bacterial MinCDE system and spatial regulation of the Z-ring. *Annu. Rev. Biochem.*, 76:539–562, 2007.

[21] Laura L Lackner, David M Raskin, and Piet AJ de Boer. ATP-dependent interactions between *Escherichia coli* Min proteins and the phospholipid membrane *in vitro*. *Journal of bacteriology*, 185(3):735–749, 2003.

[22] Tim H Szeto, Susan L Rowland, Cheryl L Habrukowich, and Glenn F King. The MinD membrane targeting sequence is a transplantable lipid-binding helix. *Journal of Biological Chemistry*, 278(41):40050–40056, 2003.

[23] Zonglin Hu and Joe Lutkenhaus. A conserved sequence at the C-terminus of MinD is required for binding to the membrane and targeting MinC to the septum. *Molecular microbiology*, 47(2):345–355, 2003.

[24] Zonglin Hu and Joe Lutkenhaus. Topological regulation of cell division in *E. coli*: spatiotemporal oscillation of MinD requires stimulation of its ATPase by MinE and phospholipid. *Molecular cell*, 7(6):1337–1343, 2001.

[25] David M Raskin and Piet AJ de Boer. Rapid pole-to-pole oscillation of a protein required for directing division to the middle of *Escherichia coli*. *Proceedings of the National Academy of Sciences*, 96(9):4971–4976, 1999.

[26] Joseph S Markson and Erin K O'Shea. The molecular clockwork of a protein-based circadian oscillator. *FEBS letters*, 583(24):3938–3947, 2009.

[27] Martin Loose, Karsten Kruse, and Petra Schwille. Protein self-organization: lessons from the Min system. *Annual review of biophysics*, 40:315–336, 2011.

[28] Karsten Kruse and Frank Jülicher. Oscillations in cell biology. *Current opinion in cell biology*, 17(1):20–26, 2005.

[29] Martin Loose and Petra Schwille. Biomimetic membrane systems to study cellular organization. *Journal of structural biology*, 168(1):143–151, 2009.

[30] Leland H Hartwell, John J Hopfield, Stanislas Leibler, and Andrew W Murray. From molecular to modular cell biology. *Nature*, 402:C47–C52, 1999.

[31] Martin Loose, Elisabeth Fischer-Friedrich, Jonas Ries, Karsten Kruse, and Petra Schwille. Spatial regulators for bacterial cell division self-organize into surface waves *in vitro*. *Science*, 320(5877):789–792, 2008.

[32] Elisabeth Fischer-Friedrich, Karsten Kruse, et al. Surface waves of Min proteins. *Physical biology*, 4(1):38, 2007.

[33] Giovanni Meacci and Karsten Kruse. Min-oscillations in *Escherichia coli* induced by interactions of membrane-bound proteins. *Physical biology*, 2(2):89, 2005.

[34] David M Raskin and Piet AJ de Boer. The MinE ring: an FtsZ-independent cell structure required for selection of the correct division site in *E. coli*. *Cell*, 91(5): 685–694, 1997.

[35] Anthony G Vecchiarelli, Min Li, Michiyo Mizuuchi, and Kiyoshi Mizuuchi. Differential affinities of MinD and MinE to anionic phospholipid influence Min patterning dynamics *in vitro*. *Molecular microbiology*, 93(3):453–463, 2014.

[36] Katja Zieske and Petra Schwille. Reconstitution of self-organizing protein gradients as spatial cues in cell-free systems. *Elife*, 3:e03949, 2014.

[37] Katja Zieske and Petra Schwille. Reconstitution of pole-to-pole oscillations of Min proteins in microengineered polydimethylsiloxane compartments. *Angewandte Chemie International Edition*, 52(1):459–462, 2013.

[38] Walid El-Sharoud. *Bacterial physiology*. Springer, 2008.

[39] Eugene V Koonin. A superfamily of ATPases with diverse functions containing either classical or deviant ATP-binding motif. *Journal of molecular biology*, 229(4): 1165–1174, 1993.

[40] Tim H Szeto, Susan L Rowland, Lawrence I Rothfield, and Glenn F King. Membrane localization of MinD is mediated by a C-terminal motif that is conserved across eubacteria, archaea, and chloroplasts. *Proceedings of the National Academy of Sciences*, 99(24):15693–15698, 2002.

[41] Lars D Renner and Douglas B Weibel. MinD and MinE interact with anionic phospholipids and regulate division plane formation in *Escherichia coli*. *Journal of Biological Chemistry*, 287(46):38835–38844, 2012.

[42] Eugenia Mileykovskaya, Itzhak Fishov, Xueyao Fu, Brian D Corbin, William Margolin, and William Dowhan. Effects of phospholipid composition on MinD-membrane interactions *in vitro* and *in vivo*. *Journal of Biological Chemistry*, 278 (25):22193–22198, 2003.

[43] Huaijin Zhou and Joe Lutkenhaus. Membrane binding by MinD involves insertion of hydrophobic residues within the C-terminal amphipathic helix into the bilayer. *Journal of bacteriology*, 185(15):4326–4335, 2003.

[44] Kyung-Tae Park, Wei Wu, Kevin P Battaile, Scott Lovell, Todd Holyoak, and Joe Lutkenhaus. The Min oscillator uses MinD-dependent conformational changes in MinE to spatially regulate cytokinesis. *Cell*, 146(3):396–407, 2011.

[45] Zonglin Hu, Edward P Gogol, and Joe Lutkenhaus. Dynamic assembly of MinD on phospholipid vesicles regulated by ATP and MinE. *Proceedings of the National Academy of Sciences*, 99(10):6761–6766, 2002.

[46] Sandra Ramirez-Arcos, Jason Szeto, Jo-Anne R Dillon, and William Margolin. Conservation of dynamic localization among MinD and MinE orthologues: oscillation of *Neisseria gonorrhoeae* proteins in *Escherichia coli*. *Molecular microbiology*, 46 (2):493–504, 2002.

[47] Jason Szeto, Sudeep Acharya, Nelson F Eng, and Jo-Anne R Dillon. The N-terminus of MinD contains determinants which affect its dynamic localization and enzymatic activity. *Journal of bacteriology*, 186(21):7175–7185, 2004.

[48] Katja Zieske, Jakob Schweizer, and Petra Schwille. Surface topology assisted alignment of Min protein waves. *FEBS letters*, 588(15):2545–2549, 2014.

[49] Simon Kretschmer and Petra Schwille. Toward spatially regulated division of protocells: insights into the *E. coli* Min system from *in vitro* studies. *Life*, 4(4):915–928, 2014.

[50] Jason Szeto, Nelson F Eng, Sudeep Acharya, Marc D Rigden, and Jo-Anne R Dillon. A conserved polar region in the cell division site determinant MinD is required for responding to MinE-induced oscillation but not for localization within coiled arrays. *Research in microbiology*, 156(1):17–29, 2005.